ACS NANO

www.acsnano.org

ARTICLE

Correlative Raman–Voltage Microscopy Revealing the Localized Structure–Stress Relationship in Silicon Solar Cells

Tianyu Lan, Tianyi Zhao, Yan Liu, Jingyu Cao, Wenqi Li, Jie Yang, Xinyu Zhang, Yusheng Wang,* and Baoquan Sun*

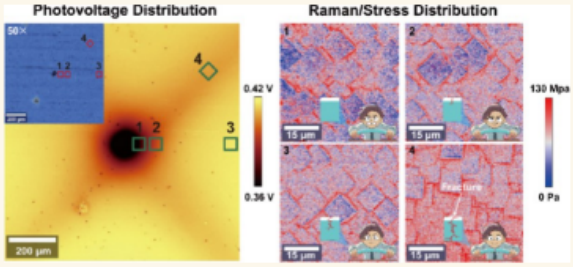
Cite This: *ACS Nano* 2025, 19, 4473–4483

Read Online

ACCESS | Metrics & More | Article Recommendations | Supporting Information

Downloaded via SOOCHOW UNIV on June 4, 2025 at 03:12:22 (UTC).
See https://pubs.acs.org/sharingguidelines for options on how to legitimately share published articles.

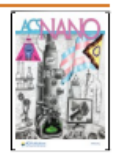
ABSTRACT: **Knowledge of localized strain at the micrometer scale is essential for tailoring the electrical and mechanical properties of ongoing thinning of crystal silicon (c-Si) solar cells. Thinning c-Si wafers below 110 μm are susceptible to cracking in manufacturing due to the nonuniform stress distribution at a micrometer region, necessitating a rigorous technique to reveal the localized stress distribution correlating with its device electrical output. In this context, a Raman microscopy integrated with a photovoltage mapping setup with high resolution to the submicrometer scale is developed to acquire correlative Raman–voltage of the localized physical properties at the microcracks on the rear side of c-Si solar cells. By integrating photoelectrical, mechanical, and theoretical simulations, we elucidated the evolution of the microcracks. The localized stresses cause significant electrical output degradation in c-Si solar cells. In addition, theoretical simulations and experimental characterization indicate that the etched rear side acts as a more intense stress concentrator, resulting in an asymmetrical stress distribution between the rear and front sides of c-Si solar cells. This finding provides valuable insights into the origin of microcracks in c-Si solar cells and serves as a metrology tool for microscale mapping of strain-engineered photovoltaic modules.**



KEYWORDS: *solar cells, microcracks, localized stress, photovoltage and photocurrent, Raman microscopy*

The global solar photovoltaic (PV) market has experienced a rapid expansion. By the end of 2023, the global installed capacity had surpassed 1 TW, with an annual capacity of 235.8 GW, thus establishing a record.[1] The pursuit of high-efficiency and cost-effective solar energy conversion is triggering the development of advanced PV technologies, focusing on manufacturing thin crystal silicon (c-Si) wafers for tunnel oxide passivated contact (TOPCon) and heterojunction solar cells.[2,3] The transition to thinning wafers represents a strategic move with the dual objective of enhancing production capacity and reducing the overall cost of c-Si solar cells and modules. The 2022–2023 International Technology Roadmap for PVs indicates that the average thickness of n-type c-Si wafers for TOPCon solar cells in 2022 is below 160 μm.[4] The rate of wafer thinning has exceeded expectations below 120 μm and is projected to continue declining in the future. Nevertheless, this ongoing thinning wafer faces significant challenges.[5] First, the Lambertian limit stipulates that the absorption of solar light is directly proportional to the width of the cell. To ensure the high-efficiency harvesting of the photons with an energy larger than 1.1 eV, the thickness of textured c-Si should be over 110 μm.[6] The pyramidal textured c-Si remains the optimal choice, although the textured surface would inevitably lead to a stress concentration. The inclination toward using thinner wafers burdens the susceptibility to mechanical stress, raising the risk of cracking during manufacturing. Such defects can significantly impair the performance and reliability of c-Si solar cells.[7] In essence, fractures in c-Si wafers during processing, handling, and transportation would expand the cracks already present in the wafers.[8] As wafer thickness is thinned to 110 μm, monitoring stress distribution as well as microcracks in PV modules becomes crucial for guaranteeing the quality and longevity of PV panels.[9,10]

Received: September 28, 2024
Revised: January 12, 2025
Accepted: January 13, 2025
Published: January 24, 2025



ACS Publications

© 2025 American Chemical Society

https://doi.org/10.1021/acsnano.4c13688
ACS Nano 2025, 19, 4473–4483

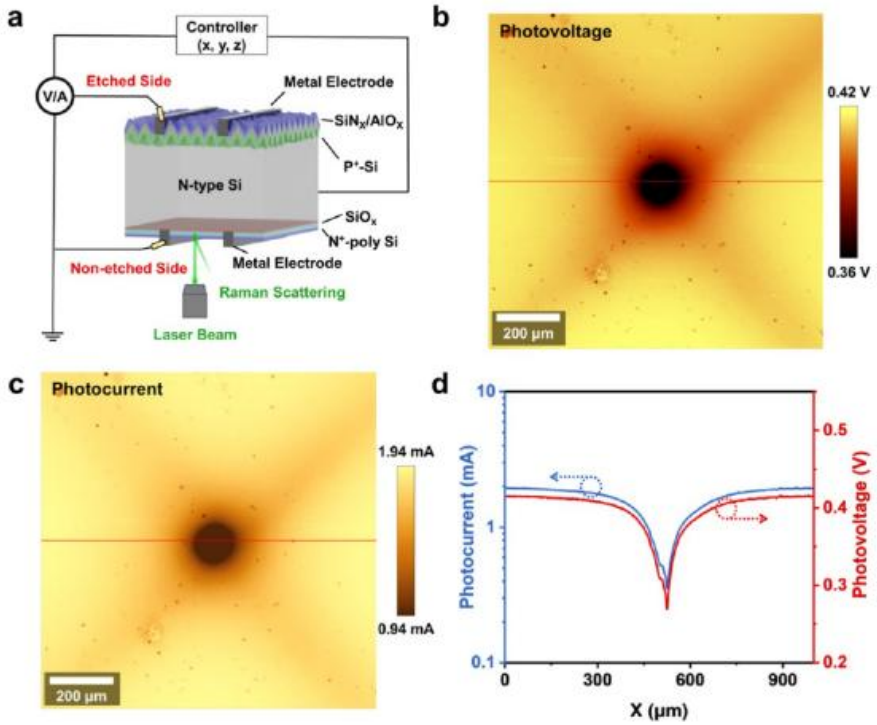


Figure 1. Photovoltage and photocurrent mapping of microcracks based on the micro-Raman spectroscopy integrated with voltage and current setup. (a) Setup diagram for photovoltage and photocurrent mapping based on Raman spectroscopy with the structure of a c-Si solar cell; photovoltage (b) and photocurrent (c) mapping around the microindent; (d) photovoltage and photocurrent collected in (b,c) of the cross-sectional image line along the center red line. The left *y*-axis denotes the photocurrent, while the right *y*-axis denotes the photovoltage.

Nowadays, the most common ways utilized to probe microcracks in c-Si solar cells, such as photoluminescence (PL), electroluminescence (EL), and laser beam-induced current imaging, have been instrumental in identifying cracks and defects.[11−13]

These microcrack detection methods generally cannot realize a high spatial resolution, primarily achieving crack monitoring at a macroscopic scale. In prior studies on microcracks in c-Si solar cells, the highest spatial resolution was only 400 μm, which limits the ability to conduct detailed investigations of microcracks.[14] Particularly in the ongoing trend toward thinner c-Si solar cells, wide attention has been paid to ultrathin silicon cells to unveil the distribution of localized stresses. However, most of these studies employ a combination of computational simulations and macroscopic characterization techniques on a hundred-micrometer scale to investigate the mechanical properties, which, by nature, provide insufficient information on the origin of the microcrack formation mechanism.[15,16] Furthermore, many researchers utilize transmission electron microscopy (TEM) to examine microcracks, allowing for the direct visualization of local stress and strain distributions.[17] However, this approach required a complicated TEM sample preparation process to facilitate the atom mapping and gain insight into substrate stress distribution, which cannot reveal the in situ stress distribution in an actual device. The TEM sample preparation process is highly likely to alter the stress distribution. All these techniques offer high sensitivity to cracks but either lack limited spatial resolution or fail the direct correlation of microcracks and electrical output. Consequently, the investigation of localized cell stresses needs to be urgently addressed. Raman spectroscopy enables monitoring localized stresses via probing Raman shifts.[18] c-Si exhibits a strong Raman peak at 520.7 cm^{-1}, corresponding to the standard transverse optical (TO) phonon mode. Furthermore, the Raman shift of the wavenumber of the c-Si TO mode peak strongly correlates with the strength of the residual localized stress. A higher wavenumber implies localized compressive stresses, while the lower wavenumber shift suggests localized tensile ones.[19] Meanwhile, Raman microscopy mapping can enable a spatial resolution up to the submicrometer, reaching the optical Rayleigh diffraction limit. As a result, Raman microscopy should be a practical tool for characterizing the stress distribution of c-Si solar cells.[20,21] However, the present Raman characterization cannot provide the correlative electrical output characteristics at the point with the residual localized stress.

Here, the correlative Raman−voltage of the localized physical properties at microcracks is acquired by Raman microscopy integrated with a photovoltage mapping setup. We demonstrate that Raman microscopy allows direct, noninvasive, and high spatial-resolved mapping of the localized residual stress in c-Si solar cells at a submicrometer scale. With a spatial resolution of approximately 300 nm, it enables us to extract localized photovoltage and stress distributions corresponding to microcracks at identical spatial coordinates. Furthermore, theoretical simulations are conducted to analyze the localized stress distribution of c-Si solar cells under bending or in a thermal field. Notably, the etched rear side exhibits a more pronounced stress concentration. By

https://doi.org/10.1021/acsnano.4c13688
ACS Nano 2025, 19, 4473−4483

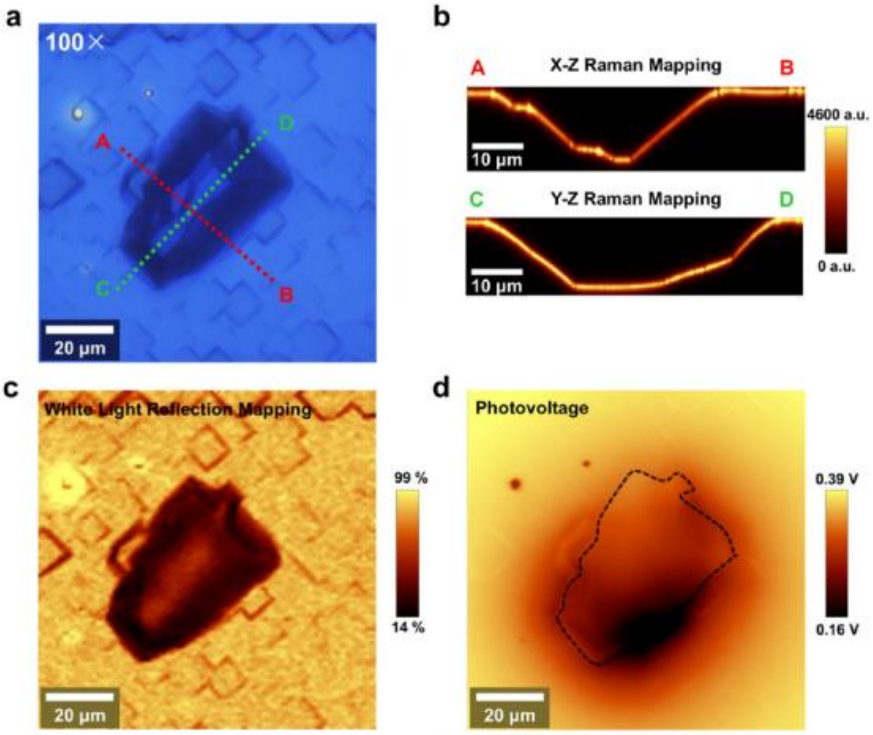


Figure 2. Characterization of microindent in the same region with different probe techniques. (a) Optical microscopy image (100×). The dashed lines AB and CD represent the routes in (b); (b) section morphology diagram by Raman intensity mapping lines shown in (a); (c) reflection mapping image under white light illumination; and (d) photovoltage mapping image (the dashed line shows the microindent profile) in the centered microindent region.

integrating photoelectrical, mechanical characterization, and theoretical simulations, we elucidated the evolution of microcracks. The localized stresses incur significant electrical output degradation in c-Si solar cells. This finding sheds light on the origin of microcracks in c-Si solar cells and provides a tool for microscale mapping of localized stress in PV modules.

RESULTS AND DISCUSSION

Raman Spectroscopy Integrated Photovoltage Mapping Setup. The photovoltage−photocurrent mapping system based on Raman microscopy to characterize c-Si solar cells is illustrated in Figure 1a. Raman microscopy is a noninvasive technique that can tailor the chemical structure, phase, stress, and defect properties of materials.[22] While traditional Raman microscopy can realize high spatial resolution by optimizing the optical pathways, it is hard to acquire the correlation between the physical properties and electrical output.[23] In this case, our system enables the probe of localized residual microcracks in the c-Si solar cells. The setup comprises a confocal Raman imaging system with solid-state lasers as the pumping source. The penetration depth of the laser in c-Si varies with its wavelength, allowing for probing of different depths of the bulk materials with a spatial resolution of approximately 300 nm. The key idea is to combine Raman microscopy with the ability to monitor photovoltage/photocurrent responses. This combination allows us to simultaneously monitor microstructural features (using Raman spectroscopy) and electrical output (measuring the photovoltage/photocurrent). The characterization method by scanning a laser beam across the c-Si wafer in a grid-like pattern can generate a two-dimensional image of Raman spectra, revealing the variations in c-Si stress. Concurrently, a corresponding optical−electrical properties image can be constructed by collecting the photovoltage/photocurrent responses at an identical region.[24] Potential correlations between the microcracks and the electrical output can be identified by comparing and correlating these two mapping images from the identical region. This approach can provide valuable insights into the relationship between microstructural stresses and electrical output in c-Si solar cells.

Photoelectrical Characterization at the Centered Region. The thickness of c-Si was 120 μm with the front p^+ emitter layer and the rear n^+ poly-Si passivating layer to build the TOPCon solar cell. The c-Si doping concentration was approximately 1×10^{20} cm^{-3}. A preliminary PL inspection revealed the presence of numerous diagonal-stripe-type dark regions (as illustrated in Figure S1, Supporting Information) on the rear side of the TOPCon solar cell. The severe photoelectric loss regions identified in the photovoltage and photocurrent images (Figure 1b,c) were assigned to the diagonal stripes observed in the PL measurements, indicating a strong correlation between these defects and the observed electrical output losses. The cross-sectional lines in Figure 1d were extracted from Figure 1b,c, which displayed the spatial distributions of photovoltage and photocurrent. The photocurrent in the microindent center was only approximately 18.3% of that of the edge one, while the photovoltage was approximately 64.8% of the edge one. An equivalent circuit

https://doi.org/10.1021/acsnano.4c13688
ACS Nano 2025, 19, 4473−4483

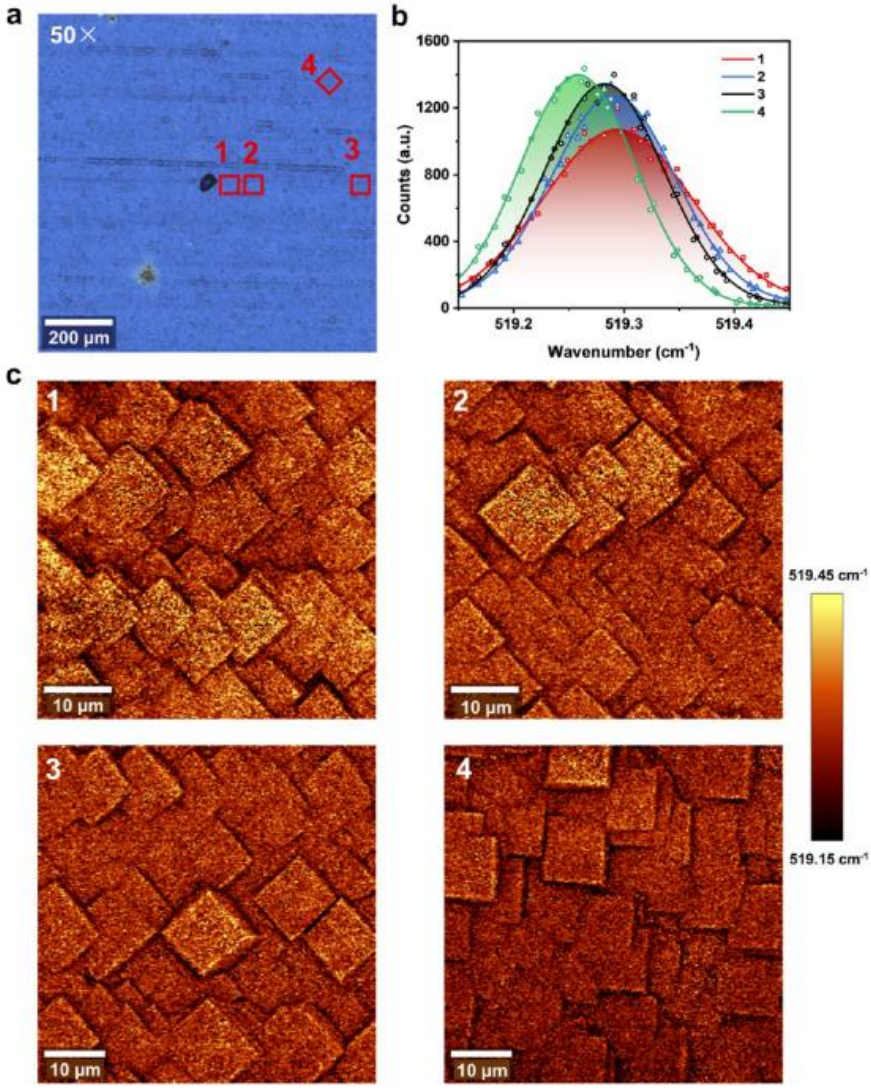


Figure 3. Localized stress characterization by Raman spectroscopy. (a) Optical microscope image (50×); (b) Raman vibration frequency statistics in the labeled regions; (c) Raman shift mapping image of the silicon TO mode located at the different regions. Detailed Raman shift mapping images for the regions labeled 1, 2, 3, and 4 in (a). The Raman shift values are displayed in wavenumbers (cm^{-1}), with the color bar indicating the shift range from 519.15 to 519.45 cm^{-1}.

diagram of the test circuit is plotted to interpret the extracted current−voltage ($I-V$) curve, as shown in Figure S2 (Supporting Information). This diagram illustrates that the photocurrent of the test corresponds to the external circuit current with a load of 1000 ohms. The $I-V$ curve in this double-diode model follows the equation

$$I = I_{ph} - I_{01}\left[\exp\frac{q(V - IR_S)}{k_B T} - 1\right] - I_{02}\left[\exp\frac{q(V - IR_S)}{2k_B T} - 1\right] - \frac{V - IR_S}{R_{Sh}} \quad (1)$$

where I_{ph} is the light-generated current, I_{01} and I_{02} symbolize the reverse saturation current of diodes 1 and 2, and R_S and R_{Sh} represent the series and the shunt resistances, respectively.[25]

Simultaneously, the photovoltage represents the cell voltage in the open-circuit state. Thus, the photocurrent and photovoltage can be converted to each other simply by transforming the logarithmic number. Additionally, we observed that the losses in photovoltage and photocurrent increase as the proximity to the microindent decreases. The photocurrent region saturates at a distance of 500 μm from the center of the microindent. In addition, the current density−voltage ($J-V$) curve and power conversion efficiency (PCE) mapping image were extracted, as shown in Figure S3. The stress-induced microindent significantly undermines the c-Si device efficiency. It yields a PCE of only 21.74% for the device with the presence of the microindent. We observed a 150 μm-diameter region where almost half of the PCE of the responded device was lost. Based on the above characterization results, we deduced that

https://doi.org/10.1021/acsnano.4c13688
ACS Nano 2025, 19, 4473−4483

the electrical properties around the microindents are responsible for the degradation of the device's electrical output.

To gain insight into the physical properties in the vicinity of the microindents, we conducted high-resolution photoelectric characterization of the microregion (100 × 100 μm^2) centered on the microindent, as depicted in Figure 2. The three-dimensional (3D) topographic image around the microindent was captured by a 100× objective and processed by a stacking method (see Figure 2a), which is identical to the site determined by the scanning electron microscope images in Figure S4 (Supporting Information). Raman depth mapping measurement was conducted to explore the inner structure of the microindent, as shown in Figure 2b. The dashed lines AB and CD represent the scanning profile in Raman mapping. The microindent presents a stepped structure inside with a height of approximately 14 μm. We employed white light as the excitation source to acquire white light reflection spectra at an identical location. The light reflection mapping image clearly illustrated the reflection characteristics of this region within the visible spectrum, as shown in Figure 2c. It reveals that the morphology of the pyramid bases significantly impacts light reflection properties. Specifically, we observed a suppressed reflection ratio at the edges of the pyramid bases, indicating an enhanced light absorption in these areas. In Figure 2d, a photovoltage mapping was performed on the same region with a 300 nm spatial resolution. The presence of microindents would influence the correspondent photovoltage. A stronger photovoltage was observed at the edge of the pyramid base in the flat region far from the microindent. This indicates that the region with more light absorbed should deserve a larger photovoltage. Conversely, around the edges of the microindents, the photovoltage is lower in the region where more light is harvested. This phenomenon is inconsistent with the fact that enhanced photovoltage originates from light absorption. Furthermore, the dashed line in Figure 2d indicated that the microindent actual profile was unlined with the photovoltage loss region. Charge recombination incurs a negative effect on photovoltage loss in c-Si solar cells.[26] Therefore, we postulated that the electrical output loss was attributed to the charge recombination instead of light loss due to the microindent. Additionally, the origin of the microindents should be inherited from nonuniform stress distribution in the wafer fabrication process. In the c-Si silicon cell fabrication process, defects with concentric circles can be detected through EL testing. The essence of the concentric circle phenomenon is the uneven distribution of impurities, and oxygen would precipitate into oxygen rings. Specifically, one of the most unavoidable impurities in c-Si is oxygen.[27] These uneven oxygen defects remaining in c-Si can affect the stability of the crystal structure, incurring significant internal stress. The subsequent c-Si wafer ingot-cutting process would cause a significant stress concentration inside the silicon wafer. The residual oxygen precipitate defects are more likely to form stress concentration spots. These spots propagate during the c-Si solar cell fabrication process. In texturing the c-Si substrates, the boron-silica glass formed during boron thermal diffusion was removed by a HF solution. Then, the samples were immersed in an alkali solution.[28] It can be postulated that the spots with high localized stress display enhanced chemical active energy. During the etching process, the localized chemical instability is highly likely to incur localized over-etching, and the microindents are formed accordingly in this way.

Raman Microscopy Spectra Near the Microindent. The photoelectric losses in the center of the microindent were ascribed to charge recombination losses. In addition, photoelectric losses along the diagonal of the microindent were observed. This morphology mimics the crossed microcracks, also known as diagonal microcracks.[29] Even using a 100× objective microscope, it was impossible to figure out a diagonal microcrack on the c-Si substrate. Since the diagonal microcrack cannot be characterized by a normal optical microscope, Raman spectrum microscopy measurements were conducted to probe crossed microcracks. The penetration depth can be modulated by utilizing different wavelength lasers. Here, a 532 nm laser with a penetration depth of 1.3 μm for c-Si was used. On the one hand, the intensity of Raman scattering is inversely proportional to the fourth power of the wavelength, necessitating the employment of lasers with lower wavelengths to ensure signal strength. On the other hand, the absorption spectrum of c-Si exhibits significant absorption in the ultraviolet region. Consequently, after a thorough evaluation, a 532 nm laser was selected as the excitation source, balancing the need for low-wavelength excitation with the limitations imposed by c-Si absorption characteristics. We characterized the photoelectric loss regions using Raman spectroscopy, ranging from 50 × 50 μm^2, to explore the physical properties of the regions. The topography of the four regions can be observed under a 50× optical microscope image, as shown in Figure 3a. The photovoltage mapping image can be divided into four regions (1, 2, 3, and 4) according to its photovoltage image. In Figure 3a, Region 1 was identified as being close to the microindent, demonstrating the most substantial degradation features in the photovoltage. Less degradation was observed in Region 2, located slightly away from the microindent. Region 3 was intentionally selected within the area characterized by nondegraded photovoltage. Finally, Region 4 was strategically positioned along the diagonal axis from the indented center, where obvious voltage degradation was probed. Figure 3b displays the c-Si TO vibration frequency distributions at the regions. As can be observed in the diagrams, the peak of c-Si shifts from the standard position (520.70 cm^{-1}) downward to the range of 519.15−519.45 cm^{-1}. Compressive uniaxial stress generally leads to a Raman blue shift, while tensile stress causes a red shift in the TO phonon mode. Although Raman shifts can be influenced by various physical factors, including stress and doping concentration variations,[30] the observed Raman shift is more likely to be ascribed to localized tensile stress rather than doping heterogeneity. The doping concentration on the rear surface of the TOPCon solar cell should be uniform following the alkaline etching process.[31] This uniformity is achieved by utilizing the LPCVD technique to deposit the backside polysilicon layer. The LPCVD process, conducted under stringent low-pressure and elevated-temperature conditions, facilitates the formation of a uniformly distributed thin film. After the deposition, the doping concentration is subjected to meticulous analysis to ascertain its uniformity across the layer. Furthermore, the high-temperature phosphorus diffusion process reinforces the uniformity of the doping profile throughout the entire specimen. In addition, the probe pump laser used in our experiments penetrates approximately 1.3 μm into the c-Si substrate. Because the thickness of the backside polysilicon layer is approximately 100 nm, it is an order of magnitude lower than the laser penetrating depth in c-Si. Therefore, most of the Raman signal should be derived from

https://doi.org/10.1021/acsnano.4c13688
ACS Nano 2025, 19, 4473−4483

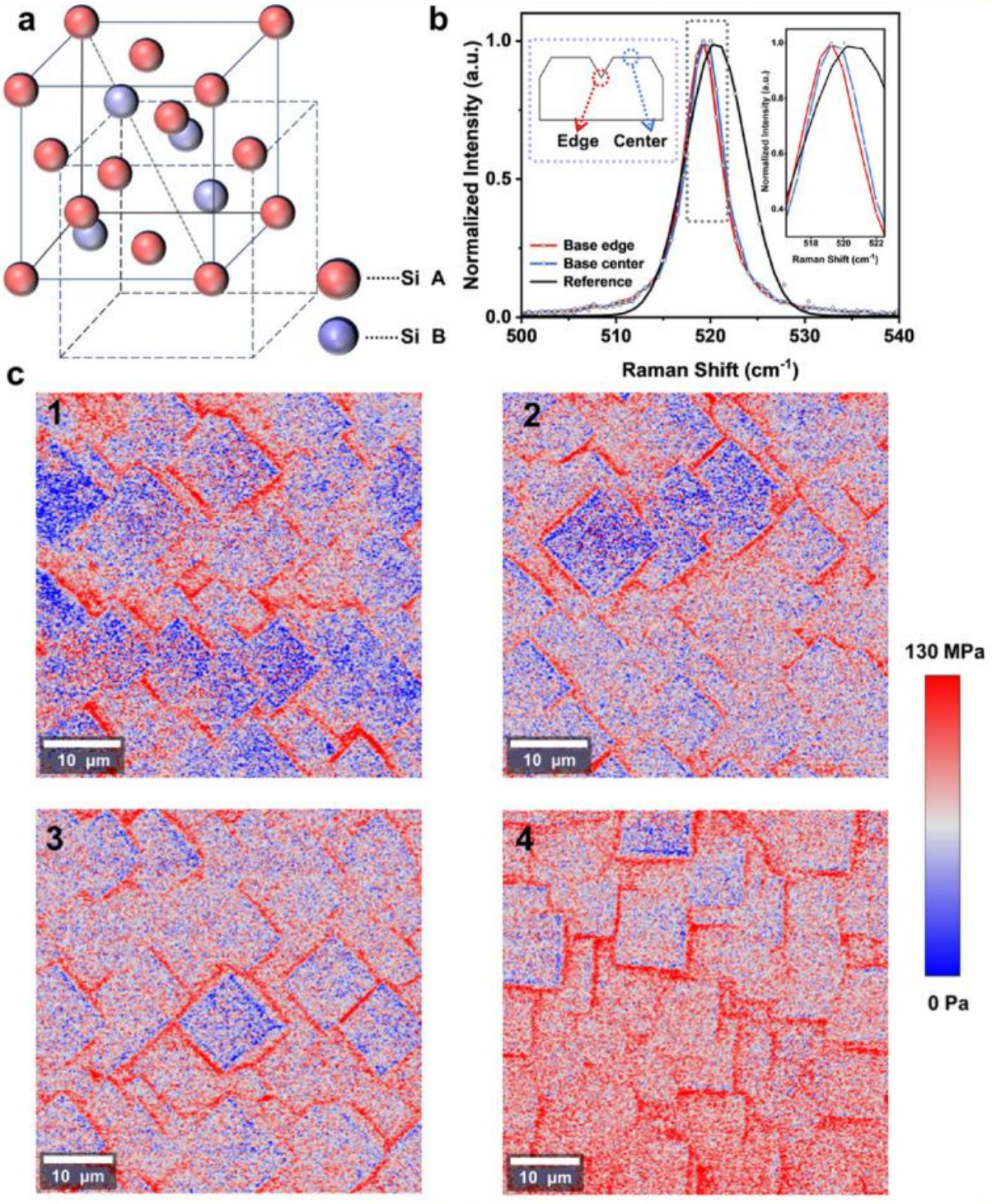


Figure 4. Correlation of c-Si Raman spectroscopy with stress distribution. (a) Scheme of lattice unit cells of single c-Si (red dots represent Si A, and green dots represent Si B); (b) Raman spectra of the TO mode monitored the different textured c-Si regions with the diagram of base center and edge. The right inset shows the enlarged spectra; and (c) localized relative stress distribution extracted from the Raman shift image of the corresponding regions 1, 2, 3, and 4 in Figure 3.

the bulk c-Si, thereby reflecting the properties of the bulk material rather than those of the polysilicon layer. Consequently, the doping concentration on the rear surface is a less discernible factor influencing the Raman shift. The descending

https://doi.org/10.1021/acsnano.4c13688
ACS Nano 2025, 19, 4473−4483

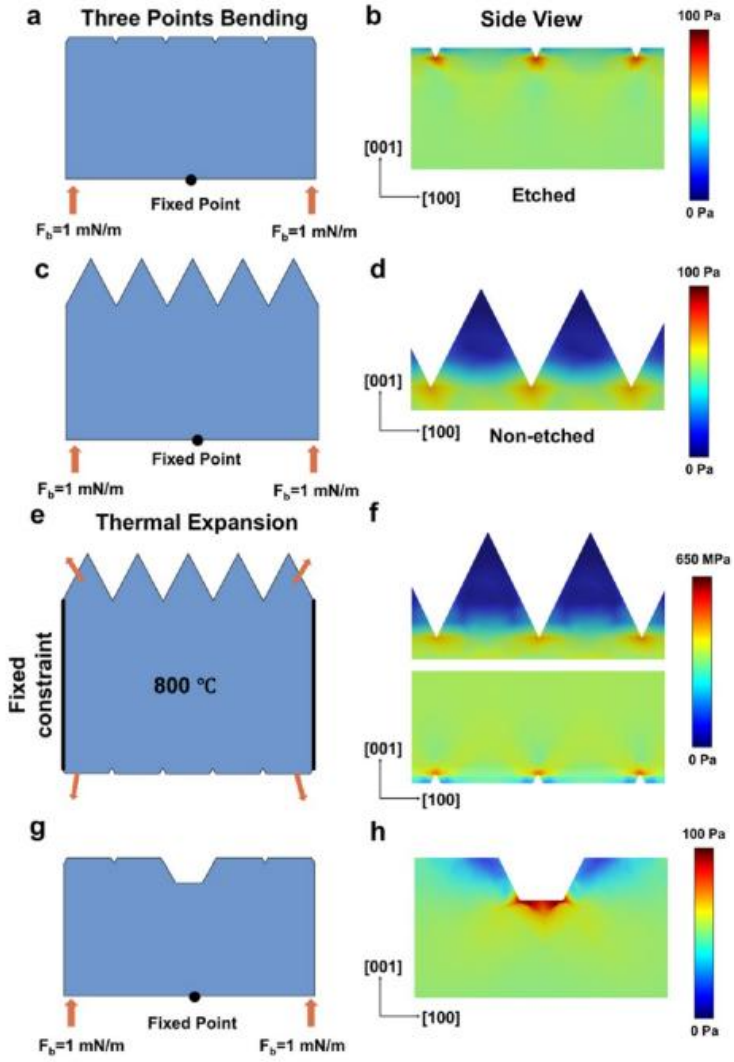


Figure 5. Localized stress simulation of c-Si solar cells by COMSOL Multiphysics. 3D simulation diagrams of the textured c-Si wafers with (a) etched, (c) nonetched, and (g) nonetched with a microindent; vertical forces F_b = 1 mN m^{-1} were applied at both wafer sides, while the middle was fixed to exclude rigid-body displacement. And the corresponding localized stress distribution in the *XZ* plane of the (b) etched, (d) nonetched surfaces, and (h) nonetched with a microindent. (e) 3D thermal stress simulation diagram of the c-Si wafer with a textured front surface and etched rear surface at a thermal annealing process of 800 °C. The corresponding localized thermal stress distribution with a textured front surface and an etched rear surface in the *XZ* plane is shown in (f).

Raman shift indicates that c-Si is under a tensile stress. The greater the shift observed, the larger the tensile stress would concur. Detailed frequency distributions in four regions are plotted in Figure 3c. The most remarkable trend of these curves is that Region 4 exhibited a lower vibration frequency (~519.25 cm^{-1}), meaning c-Si in this region has a larger shift than the standard mode. From this, we deduced that c-Si in Region 4 suffered the most significant tensile stress. These variations suggest that black Region 1 has a higher vibrational energy (~519.30 cm^{-1}) and less extensive tensile stress. Region 3 exhibits lower vibrational energy (~519.28 cm^{-1}) and larger tensile stress, with Region 2 displaying intermediate characteristics (~519.29 cm^{-1}). According to the relationship between Raman shift and localized stresses, it can be inferred that the stresses in the region closer to the microindent are much smaller, which is as unplausible as we expected. The region of the microindent would be expected to have the highest localized stress. The surrounding region away from the microindent should display slightly lower localized stress. However, the lowest stress was monitored in our experiment results. To understand this phenomenon, we subsequently conducted relevant theoretical simulations. Furthermore, the morphology of the pyramid base impacts the distribution of the localized stresses. The stresses exhibit a relatively small tensile stress distribution over the face area of the pyramid base, whereas an inverse, more extensive tensile stress distribution concurs at the edges. It has been reported that microcracks represent the most prevalent form of stress concentration in c-Si wafers.[32] In the vicinity of these microcracks, local stresses are considerably higher than those

https://doi.org/10.1021/acsnano.4c13688
ACS Nano 2025, 19, 4473−4483

observed at the macroscopic level, making them challenging to release. When stress levels overpassed the critical threshold, microcracks would concur.[33] Consequently, we postulate that stress-concentrated cracks occur in the central region around the microindents and propagate along the c-Si wafer, forming crossed microcracks. Once the microindent is generated, all the accumulated stress in c-Si would be released.

Furthermore, the c-Si phonon mode is investigated to gain insight into the distribution of the localized stress. Concerning c-Si, as illustrated in Figure 4a, it has a unit cell of the diamond lattice. This comprises two overlapped face-centered cubic crystal unit cells, offset by one-quarter along the diagonal of a cubic cell. Each primitive cell contains two atoms designated A (0, 0, and 0) and B (1/4, 1/4, and 1/4). Consequently, four distinct phonon modes are obtained regarding a 3D double-atom chain vibration mode.[34] The vibration can be described by the following waves: TO, longitudinal optical (LO), longitudinal acoustic, and transverse acoustic. Optical waves display higher frequencies than acoustic waves, which makes them more likely to couple with photons and generate Raman scattering. Furthermore, the two transverse vibration modes are identified in a cubic crystal system, which results in the 2-fold degenerate nature of transverse waves in c-Si. The TO and LO modes degenerate in the central Brillouin zone, resulting in an intense triple degenerate mode (ω_1, ω_2, and ω_3) at 520.7 cm^{-1}. Figure 4b presents the Raman spectra of c-Si measured in different situations. The left inset diagram displays the positions measured in the spectra. The reference line represents a standard c-Si Raman spectrum with a TO mode of 520.69 cm^{-1}. The Raman spectra of c-Si in the pyramid base center (~519.45 cm^{-1}) and edge (~519.15 cm^{-1}) exhibit a downward shift in wavenumber, as shown in the right inset. The device substrate shift deviation from a standard mode of c-Si to ~519 cm^{-1} can be ascribed to c-Si doping concentration altering the Raman position. Conversely, the Raman mode of c-Si located at the adjacent pyramid edges exhibits a lower Raman shift than the pyramid one. The Raman shift distinction elucidates nonuniform localized stress distribution. In particular, the frequency (ω) of the c-Si Raman peak of the degenerate mode shifts with hydrostatic pressure. The frequencies are

$$\omega_1 = \omega_2 = \omega_3 = \omega_R + \frac{\omega_R}{2}(p + 2q)\eta \quad (2)$$

Here, the values of ω_1, ω_2, and ω_3 are equal to that of ω because frequency is 3-fold degeneracy. ω_R means the frequency of the 3-fold degeneracy TO mode (stress free value). p and q are material-independent elements, the so-called phonon deformation potentials. n Represents Lagrangian finite strain parameters. For c-Si, p and q are -0.385×10^{28} dyn cm^{-1} g^{-1} and $q = -1.036 \times 10^{28}$ dyn cm^{-1} g^{-1}, respectively.[35] With these parameters, the equation can be simplified by $\omega = -2.29 \times 10^{-9}\ \sigma$. Here, σ represents the uniaxial stress. To directly display the localized stress distribution between the pyramid face and the edge one, the relative stress distribution against the Raman shift was extracted from Figure 3c, as shown in Figure 4c. The diagrams illustrate that the maximum localized relative stress is about 130 MPa. It can be concluded that the diagonal region exhibits the greatest difference in localized relative stress. Despite their similar morphological characteristics, significant localized stress was observed in the diagonal regions, correlating with a notable degraded photoelectrical loss. Consequently, it is concluded that the primary factor determining the photoelectric loss is ascribed to localized tensile stress.

Mechanical Analysis of Asymmetric Structures in c-Si Solar Cells. As discussed above, the pyramidal base structure critically affected the stress distribution. To interpret the localized stress distribution collected by Raman mapping, we used COMSOL Multiphysics to simulate the localized stress distribution in the c-Si pyramid base morphology under external stress loads. This simulation explored the correlative effect on surface morphology versus the localized stress distribution. A 3D simulation of an etched c-Si wafer is depicted in Figure 5a. Three points were fixed on the upper surface near the middle of the wafer to exclude rigid-body displacement. Bending forces of 1 mN m^{-1} were applied on both sides of the wafer. The results of the localized stress distribution in the XZ plane upon application of the bending loads are shown in Figure 5b. It can be observed that significant stresses are present at the grooves, with less localized stresses within the faces. This observation is consistent with previous studies on foldable flexible c-Si solar cells, where localized stress concentrates within the narrow channels separating the pyramidal structures under bending forces.[17] Congruent results of COMSOL simulations and microscopic investigations confirm that the tensile stress concentration concurs at such critical edge locations. The findings demonstrate a significantly lower stress distribution at the pyramid base center region and a more extensive stress distribution at the edge. Therefore, it can be inferred that a local tensile stress distribution is centered around the etching residual microindents and propagates along the c-Si [110] crystallographic direction. This localized tensile stress incurs an electrical output degradation.

Furthermore, the influence of nonetched and etched surface structures on the front and rear facets of c-Si solar cells was explored to map the distribution of localized stress. A vertical force of 1 mN m^{-1} was applied meticulously at the termini of the c-Si wafer, thereby mimicking a realistic mechanical environment, as depicted in Figure 5c. The distribution of localized surface stress within the XZ plane, as illustrated in Figure 5d, indicated a predominant accumulated stress within the edges of the surface structures, which lined well with those of previous studies.[17] The localized stress within adjacent regions between the pyramid on etched c-Si surfaces is more readily observable than in nonetched ones. Our simulation showed an accumulated stress concentration on the rear side surface. Furthermore, Figure S5 (Supporting Information) illustrates the stress distribution within the XY plane of nonetched and etched structures. This demonstrates that stress concentration is primarily located between the edges, where the etched structures exhibit a higher stress concentration. This finding indicates that within the structural framework of c-Si cells, the rear side (etched) is vulnerable to accumulating localized stress under bending forces compared to the front one (nonetched), rendering the former more susceptible to fracturing under such conditions. Furthermore, a thermal stress simulation was conducted for quantitative analysis under a temperature of 800 °C, as depicted in Figure 5e.[36] The thermal stress distribution, depicted in Figure 5f, reflects the localized tensile stress distribution with accumulated stress at the edges. The etched c-Si surface exhibited a markedly higher thermal stress concentration up to 650 MPa. The magnitude of stress generated from the thermal annealing process by the simulation method is lined well with that observed from the

https://doi.org/10.1021/acsnano.4c13688
ACS Nano 2025, 19, 4473−4483

experiment (~130 MPa). Consequently, this simulation indicates that the rear side of c-Si solar cells is vulnerable to trigger cracks due to a more extensive localized stress distribution than the front one under thermal loads. The asymmetry on the front and rear sides of c-Si solar cells incurs stresses more concentrated on the rear side. The localized stress concentration on the etched rear side of c-Si solar cells corresponds to subsurface defects that limit the fracture strength of c-Si wafers.[37]

In addition, the localized stress distribution surrounding the microindent was explored. The stress shows an ascending trend along the [100] crystallographic direction from the microindent, as shown in Figure 5g,h. Meanwhile, the [110] crystallographic direction exhibits the highest stress distribution, as shown in Figure S6a (Supporting Information). Through the above analysis, a microindent mode can be visualized. Localized stress grows progressively from Regions 1, 2, to 3, as shown in Figure 4, while the area near the microindent experiences the minimum local stress. These phenomena can be interpreted by stress release. The pyramid base edge accumulated stress when forming the microindent in the etching process. Localized stress accumulation made the microindent unstable and prone to overetching. Once surpassing an etching threshold, the accumulated stress was released in association with microindent formation. Furthermore, as the thermal stress simulation shown in Figure S6b (Supporting Information), under a temperature of 800 °C, stress is distributed along the [110] direction, making microcracks propagate in this direction. Therefore, the generated microindents on the rear side of c-Si solar cells in the (100) crystal plane would make microcracks propagate quickly in the [110] direction to a centimeter scale. Therefore, the direction to avoid microindent formation should focus on the uniformity of c-Si ingot growth and wafer-cutting processes to eliminate any localized stress distribution. Otherwise, residual stress would propagate the following c-Si solar cell and module fabrication process.

CONCLUSIONS

In summary, we have achieved the corelative residual stress and electrical output simultaneously visualized by Raman−voltage microscopy probing of the rear side of the c-Si solar cells. It enables the study of stress-induced changes of the localized electrical output characters at the submicrometer scale (300 nm), which is paramount in c-Si PV technology. Our results indicated that the localized stresses incur a degradation in the electrical output. The electrical output character exhibited a significant degradation due to the presence of microindents. Furthermore, a localized tensile stress difference of 130 MPa was identified across the rear side pyramid base structure at the electrical output degradation regions. A more considerable localized thermal stress was simulated on the rear side of the c-Si solar cells. The simulated results further verified that the rear side of c-Si solar cells exhibits a higher localized stress distribution than the front side in the asymmetric structure. With experimental and simulation calculations, we deduced that the microindents on the rear side of c-Si solar cells originate from the etching process, inherited from either the ingot growth or the wafer cutting process. What exceeds our expectations is that the regions surrounding the microindent suffered minor localized stress compared to those far away. Upon the formation of microindents, the surrounding stress was released, propagating crossed microcracks in the [110] direction. Our study represents a novel approach to exploring microcracks in PV modules for stress distribution characterization from the microscale to nanoscale.

EXPERIMENTAL SECTION

Samples. The TOPCon solar cells were provided by Jinko Solar Co., Ltd. The layers comprised Ag finger contact, an SiN_x antireflection and passivating layer, a p^+ emitter, an n-type c-Si substrate, an SiO_x tunnel layer, an n^+ poly-Si passivating layer, an SiN_x antireflection layer, and Ag finger contact (as shown in Figure 1a) from top to bottom. A photovoltage/photocurrent mapping system was developed based on Raman spectroscopy.

Raman Microscopy Instrumentation. The system configuration is plotted in Figure S7 (Supporting Information) using a WITec α300R confocal Raman imaging system to perform *XY* two-dimensional Raman spectroscopy. An excitation source 532 nm laser was used. Coupled with a 100× objective, the optical system achieves a spot radius of approximately 300 nm, providing the spatial resolution of approximately 300 nm required for imaging over the *X*-axe (*Y*-axe). A region of 1 × 1 mm^2 was mapped with a 500 × 500 grid size to obtain the photovoltage and photocurrent mapping image. A stitch length of 2 μm was utilized by using a 50× objective. In addition, the centered regions were characterized by sizes of 100 × 100 and 50 × 50 μm^2 with 250,000 and 62,500 data points, using a 100× objective, respectively. A laser power of 10 mW was set, unless specified.

Theoretical Simulation. A COMSOL Multiphysics (V.6.1) instrument was applied to simulate the localized residual stress distribution. The length, width, and height of the c-Si substrate were set as 200, 10, and 100 μm, respectively. An array of 0.1 μm pyramid bases was arranged on the c-Si substrate. The top surface was textured c-Si with pyramids and etched pyramids. The Young's modulus, Poisson's ratio, and bulk density of the wafer were set as 170 GPa, 0.28, and 2.33 g cm^{-3}, respectively. Three points were fixed surrounding the center of the rear side of the c-Si wafer, and a bending force (Fb) of 1 mN m^{-1} was applied to the two end points. Additionally, thermal stress simulations were conducted under temperature vibration from room temperature to 800 °C. Both the front and rear structures of the cells were applied to simulate thermal stress. Finally, stress distribution surrounding a microindent with a side diameter of 2 μm was conducted under both bending and thermal loads.

ASSOCIATED CONTENT

Supporting Information

The Supporting Information is available free of charge at https://pubs.acs.org/doi/10.1021/acsnano.4c13688.

PL spectra, photovoltage, and photocurrent test equivalent circuit diagram of a Raman microscopy with electrical measurement setup for TOPCon solar cells; SEM image; simulated stress distributions in the *XY* plane by COMSOL Multiphysics; and Raman microscopy and photovoltage/current mapping system equipment diagram (PDF)

AUTHOR INFORMATION

Corresponding Authors

Yusheng Wang − *Jiangsu Key Laboratory for Carbon-Based Functional Materials & Devices, Institute of Functional Nano & Soft Materials (FUNSOM), Soochow University, Suzhou 215123, P. R. China*; Email: yushengwang@suda.edu.cn

Baoquan Sun − *Jiangsu Key Laboratory for Carbon-Based Functional Materials & Devices, Institute of Functional Nano & Soft Materials (FUNSOM), Soochow University, Suzhou 215123, P. R. China; Macau Institute of Materials Science and Engineering, MUST-SUDA Joint Research Center for*

https://doi.org/10.1021/acsnano.4c13688
ACS Nano 2025, 19, 4473−4483

Advanced Functional Materials, Macau University of Science and Technology, Taipa, Macau 999078, P. R. China; orcid.org/0000-0002-4507-4578; Email: bqsun@suda.edu.cn

Authors

Tianyu Lan – *Jiangsu Key Laboratory for Carbon-Based Functional Materials & Devices, Institute of Functional Nano & Soft Materials (FUNSOM), Soochow University, Suzhou 215123, P. R. China*

Tianyi Zhao – *Jiangsu Key Laboratory for Carbon-Based Functional Materials & Devices, Institute of Functional Nano & Soft Materials (FUNSOM), Soochow University, Suzhou 215123, P. R. China*

Yan Liu – *Jiangsu Key Laboratory for Carbon-Based Functional Materials & Devices, Institute of Functional Nano & Soft Materials (FUNSOM), Soochow University, Suzhou 215123, P. R. China*

Jingyu Cao – *Research and Development (R&D) Department, Zhejiang Jinko Solar Co., Ltd, Haining 314416, P. R. China*

Wenqi Li – *Research and Development (R&D) Department, Zhejiang Jinko Solar Co., Ltd, Haining 314416, P. R. China*

Jie Yang – *Research and Development (R&D) Department, Zhejiang Jinko Solar Co., Ltd, Haining 314416, P. R. China*

Xinyu Zhang – *Research and Development (R&D) Department, Zhejiang Jinko Solar Co., Ltd, Haining 314416, P. R. China*

Complete contact information is available at: https://pubs.acs.org/10.1021/acsnano.4c13688

Notes

The authors declare no competing financial interest.

ACKNOWLEDGMENTS

This work was supported by the National Key Research and Development Program of China (2023YFB4202602).

REFERENCES

(1) Masson, G.; l'Epine, M. D., Kaizuka, I. IEA PVPS Trends in Photovoltaic Applications 2023, https://iea-pvps.org/wp-content/uploads/2023/10/PVPS_Trends_Report_2023_WEB.pdf (accessed Oct, 2023).

(2) Fazal, M. A.; Rubaiee, S. Progress of PV Cell Technology: Feasibility of Building Materials, Cost, Performance, and Stability. *Sol. Energy* **2023**, *258*, 203–219.

(3) Wang, L.; Tang, Y.; Zhang, S.; Wang, F. Z.; Wang, J. Energy Yield Analysis of Different Bifacial PV (Photovoltaic) Technologies: TOPCon, HJT, PERC in Hainan. *Sol. Energy* **2022**, *238*, 258–263.

(4) Ullah, H.; Czapp, S.; Szultka, S.; Tariq, H.; Qasim, U. B.; Imran, H. Crystalline Silicon (c-Si)-Based Tunnel Oxide Passivated Contact (TOPCon) Solar Cells: a Review. *Energies* **2023**, *16*, 715–725.

(5) Dai, H.; Yang, L.; He, S. L. 50-μm Thin Crystalline Silicon Heterojunction Solar Cells with Dopant-Free Carrier-Selective Contacts. *Nano Energy* **2019**, *64*, 103930.

(6) Su, Q.; Lin, H.; Wang, G. S.; Tang, H. B.; Xue, C. W.; Li, Z. G.; Xu, X. X.; Gao, P. Q. Theoretical Limiting-Efficiency Assessment on Advanced Crystalline Silicon Solar Cells with Auger Ideality Factor and Wafer Thickness Modifications. *Prog. Photovoltaics* **2024**, *32*, 587–598.

(7) Teplin, C. W.; Lee, B. G.; Fanning, T. R.; Wang, J.; Grover, S.; Hasoon, F.; Bauer, R.; Bornstein, J.; Schroeter, P.; Branz, H. M. Pyramidal Light Trapping and Hydrogen Passivation for High-Efficiency Heteroepitaxial (100) Crystal Silicon Solar Cells. *Energy Environ. Sci.* **2012**, *5*, 8193–8198.

(8) Brun, X. F.; Melkote, S. N. Analysis of Stresses and Breakage of Crystalline Silicon Wafers During Handling and Transport. *Sol. Energy Mater. Sol. Cells* **2009**, *93*, 1238–1247.

(9) Pratt, L.; Govender, D.; Klein, R. Defect Detection and Quantification in Electroluminescence Images of Solar PV Modules Using U-Net Semantic Segmentation. *Renewable Energy* **2021**, *178*, 1211–1222.

(10) Hacke, P.; Spataru, S.; Habersberger, B.; Chen, Y. F. Field-Representative Evaluation of PID-Polarization in Topcon PV Modules by Accelerated Stress Testing. *Prog. Photovoltaics* **2024**, *32*, 346–355.

(11) Bhoopathy, R.; Kunz, O.; Juhl, M.; Trupke, T.; Hameiri, Z. Outdoor Photoluminescence Imaging of Photovoltaic Modules with Sunlight Excitation. *Prog. Photovoltaics* **2018**, *26*, 69–73.

(12) Frazao, M.; Silva, J. A.; Lobato, K.; Serra, J. M. Electroluminescence of Silicon Solar Cells Using a Consumer Grade Digital Camera. *Measurement* **2017**, *99*, 7–12.

(13) Qiu, W. C.; Hu, W. D. Laser Beam Induced Current Microscopy and Photocurrent Mapping for Junction Characterization of Infrared Photodetectors. *Sci. China Phys. Mech.* **2015**, *58*, 1–13.

(14) Dhimish, M.; Mather, P. Ultrafast High-Resolution Solar Cell Cracks Detection Process. *IEEE Trans. Ind. Inf.* **2020**, *16*, 4769–4777.

(15) Wu, T. J.; Liu, Z. L.; Lin, H.; Gao, P. Q.; Shen, W. Z. Free-Standing Ultrathin Silicon Wafers and Solar Cells through Edges Reinforcement. *Nat. Commun.* **2024**, *15*, 3843.

(16) Lee, Y.; Woo, J. H.; Kim, K.; Lee, K. S.; Jeong, Y.; Kim, J.; Hwang, G. W.; Lee, D. K.; Kim, J. Y.; Kim, I. Laser-Assisted Nanotexturing for Flexible Ultrathin Crystalline Si Solar Cells. *Sol. RRL* **2023**, *7*, 2300376.

(17) Liu, W. Z.; Liu, Y. J.; Yang, Z. Q.; Xu, C. Q.; Li, X. D.; Huang, S. L.; Shi, J. H.; Du, J. L.; Han, A. J.; Yang, Y. H.; et al. Flexible Solar Cells Based on Foldable Silicon Wafers with Blunted Edges. *Nature* **2023**, *617*, 717–723.

(18) Li, Z. L.; Deng, L. B.; Kinloch, I. A.; Young, R. J. Raman Spectroscopy of Carbon Materials and Their Composites: Graphene, Nanotubes and Fibres. *Prog. Mater. Sci.* **2023**, *135*, 101089.

(19) Wolf, I. D. Micro-Raman Spectroscopy to Study Local Mechanical Stress in Silicon Integrated Circuits. *Semicond. Sci. Technol.* **1996**, *11*, 139–154.

(20) Pogue, V.; Melkote, S. N.; Danyluk, S. Residual Stresses in Multi-Crystalline Silicon Photovoltaic Wafers Due to Casting and Wire Sawing. *Mater. Sci. Semicond. Process.* **2018**, *75*, 173–182.

(21) Huang, Y. Q.; Zeng, Y. H.; Zhang, Z.; Guo, X. Q.; Liao, M. D.; Shou, C. H.; Huang, S. H.; Yan, B. J.; Ye, J. C. UV-Raman Scattering of Thin Film Si with Ultrathin Silicon Oxide Tunnel Contact for High Efficiency Crystal Silicon Solar Cells. *Sol. Energy Mater. Sol. Cells* **2019**, *192*, 154–160.

(22) Fischer, B.; Lambertz, A.; Nuys, M.; Beyer, W.; Duan, W. Y.; Bittkau, K.; Ding, K. N.; Rau, U. Insights into the Si-H Bonding Configuration at the Amorphous/Crystalline Silicon Interface of Silicon Heterojunction Solar Cells by Raman and FTIR Spectroscopy. *Adv. Mater.* **2023**, *35*, 2306351.

(23) Ilchenko, O.; Pilgun, Y.; Kutsyk, A.; Bachmann, F.; Slipets, R.; Todeschini, M.; Okeyo, P. O.; Poulsen, H. F.; Boisen, A. Fast and Quantitative 2D and 3D Orientation Mapping Using Raman Microscopy. *Nat. Commun.* **2019**, *10*, 5555.

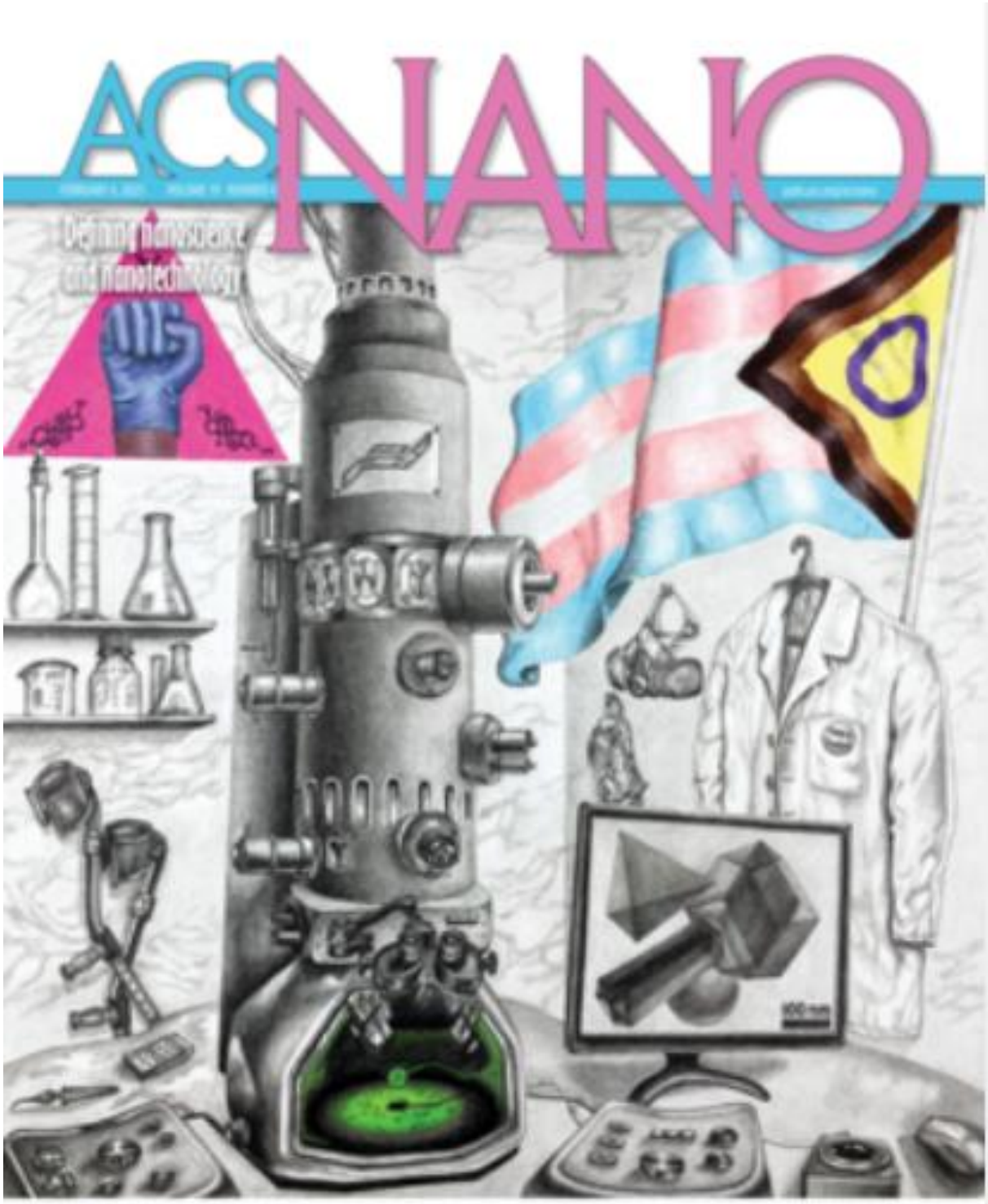
(24) Wood, S.; O'Connor, D.; Jones, C. W.; Claverley, J. D.; Blakesley, J. C.; Giusca, C.; Castro, F. A. Transient Photocurrent and Photovoltage Mapping for Characterisation of Defects in Organic Photovoltaics. *Sol. Energy Mater. Sol. Cells* **2017**, *161*, 89–95.

(25) Allam, D.; Yousri, D. A.; Eteiba, M. B. Parameters Extraction of the Three Diode Model for the Multi-Crystalline Solar Cell/Module Using Moth-Flame Optimization Algorithm. *Energy Convers. Manage.* **2016**, *123*, 535–548.

(26) Vorasayan, P.; Betts, T. R.; Tiwari, A. N.; Gottschalg, R. Multi-Laser LBIC System for Thin Film PV Module Characterisation. *Sol. Energy Mater. Sol. Cells* **2009**, *93*, 917–921.

(27) Yu, X. G.; Chen, J. H.; Ma, X. Y.; Yang, D. R. Impurity Engineering of Czochralski Silicon. *Mater. Sci. Eng. R Rep.* **2013**, *74*, 1−33.
(28) Chen, W. H.; Yu, Y. Y.; Wang, W. J.; Chen, P. H.; Ke, Y. P.; Liu, W. Q.; Wan, Y. M. Influence of Rear Surface Pyramid Base Microstructure on Industrial N-TOPCon Solar Cell Performances. *Sol. Energy* **2022**, *247*, 24−31.
(29) Borrero-López, O.; Vodenitcharova, T.; Hoffman, M.; Leo, A. J. Fracture Strength of Polycrystalline Silicon Wafers for the Photovoltaic Industry. *J. Am. Ceram. Soc.* **2009**, *92*, 2713−2717.
(30) Mastrippolito, D.; Palleschi, S.; Tosti, S.; Ottaviano, L. Doping Profiling of Beveled Si Wafers Via UV-Micro Raman Spectroscopy. *Appl. Surf. Sci.* **2021**, *567*, 150824.
(31) Ghosh, D. K.; Bose, S.; Das, G.; Acharyya, S.; Nandi, A.; Mukhopadhyay, S.; Sengupta, A. Fundamentals, Present Status and Future Perspective of TOPCon Solar Cells: a Comprehensive Review. *Surf. Interfaces* **2022**, *30*, 101917.
(32) Paul, I.; Majeed, B.; Razeeb, K. M.; Barton, J. Statistical Fracture Modeling of Silicon with Varying Thickness. *Acta Mater.* **2006**, *54*, 3991−4000.
(33) Kajari-Schröder, S.; Kunze, I.; Eitner, U.; Köntges, M. Spatial and Orientational Distribution of Cracks in Crystalline Photovoltaic Modules Generated by Mechanical Load Tests. *Sol. Energy Mater. Sol. Cells* **2011**, *95*, 3054−3059.
(34) Warren, J. L.; Yarnell, J. L.; Dolling, G.; Cowley, R. A. Lattice Dynamics of Diamond. *Phys. Rev.* **1967**, *158*, 805−808.
(35) DeWolf, I.; Maes, H. E.; Jones, S. K. Stress Measurements in Silicon Devices through Raman Spectroscopy: Bridging the Gap Between Theory and Experiment. *J. Appl. Phys.* **1996**, *79*, 7148−7156.
(36) Padhamnath, P.; Khanna, A.; Nandakumar, N.; Nampalli, N.; Shanmugam, V.; Aberle, A. G.; Duttagupta, S. Development of Thin Polysilicon Layers for Application in Monopoly Cells with Screen-Printed and Fired Metallization. *Sol. Energy Mater. Sol. Cells* **2020**, *207*, 110358.
(37) Cheng, D. M.; Gao, Y. F. A Critical Review on the Fracture of Ultra-Thin Photovoltaics Silicon Wafers. *Sol. Energy Mater. Sol. Cells* **2024**, *274*, 112999.

https://doi.org/10.1021/acsnano.4c13688
ACS Nano 2025, 19, 4473−4483



ACS Publications
Most Trusted. Most Cited. Most Read.
www.acs.org

EDITORIALS

Transdisciplinarity: Toward Trans Inclusion and Creative Artistic Expression in the Physical Sciences

Saxon Fisher*

ACS Nano 2025, 19, 4, 3947–3948 (Editorial) Subscribed
Publication Date (Web): February 4, 2025

First Page | Full Text | PDF

PERSPECTIVES

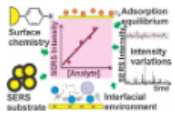
Factors that Affect Quantification in Surface-Enhanced Raman Scattering

Meikun Fan and Alexandre G. Brolo*

ACS Nano 2025, 19, 4, 3959–3995 (Perspective) Subscribed
Publication Date (Web): January 24, 2025

Abstract | Full Text | PDF

ABSTRACT



ADVERTISEMENT
DIGITAL ADVERTISING TOOLKIT
C&EN Media Group's solutions, best practices and case studies for an effective online ad strategy
c&en
Download Now

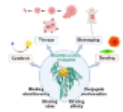
Precision Metal Nanoclusters Meet Proteins: Crafting Next-Gen Hybrid Materials

Sihan Zhang, Zhenghan Liu, Ruikuan Zhang, Qiaofeng Yao*, and Jianping Xie*

ACS Nano 2025, 19, 4, 3997–4013 (Perspective) Subscribed
Publication Date (Web): January 24, 2025

Abstract | Full Text | PDF

ABSTRACT



REVIEWS

Transforming Medicine: Cutting-Edge Applications of Nanoscale Materials in Drug Delivery

Rumiana Tenchov, Kevin J. Hughes, Magesh Ganesan, Kavita J. Iyer, Krittika Rathan, Leilani M. Lott Diaz, Robert E. Bird, Julian M. Ivanov, and Qiongqiong Angela Zhou*

ACS Nano 2025, 19, 4, 4211–4236 (Review) Open Access
Publication Date (Web): January 17, 2025

Abstract | Full Text | PDF

ABSTRACT



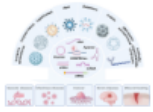
Emerging Delivery Systems for Enabling Precision Nucleic Acid Therapeutics

Xiaochun Bian, Liqing Zhou*, Zhiwei Luo, Guotao Liu, Zhongzi Hang, Haohao Li, Fengyong Li*, and Yongqiang Wen*

ACS Nano 2025, 19, 4, 4289–4309 (Review) Subscribed
Publication Date (Web): January 21, 2025

Abstract | Full Text | PDF

ABSTRACT



The Rising of Flexible Organic Electrochemical Transistors in Sensors and Intelligent Circuits

Zihan Zhu, Yunsong Pang, Yang Li*, Yuzhe Su, Xiaotian Wang, Jiaxi Yu, Baoguang Liu, Shujuan Liu, Wei Huang*, and Qiang Zhao*

ACS Nano 2025, 19, 4, 4269–4322 (Review) Subscribed
Publication Date (Web): January 20, 2025

Abstract | Full Text | PDF

ABSTRACT



Building a Better All-Solid-State Lithium-Ion Battery with Halide Solid-State Electrolyte

Chao Li and Yaqing Du*

ACS Nano 2025, 19, 4, 4121–4155 (Review) Subscribed
Publication Date (Web): January 21, 2025

Abstract | Full Text | PDF

ABSTRACT



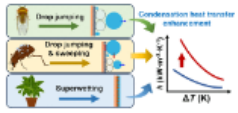
Bioinspired Superwettability Surface Strategies for Condensation Heat Transfer

Rui Wang, Yuan Tian, Botao Shen, and Xuefeng Gao*

ACS Nano 2025, 19, 4, 4156–4189 (Review) Subscribed
Publication Date (Web): January 27, 2025

Abstract | Full Text | PDF

ABSTRACT



ARTICLES

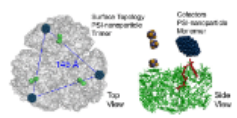
Structural Characterization of the Platinum Nanoparticle Hydrogen-Evolving Catalyst Assembled on Photosystem I by Light-Driven Chemistry

Nina S. Ponomarenko*, Nestor J. Zaluzec, Xiaoqing Zuo, Olaf J. Borkiewicz, Justin M. Hoffman, Sihan Kwon, Alex S. F. Martinson, Lisa M. Utschig*, and David M. Tiede*

ACS Nano 2025, 19, 4, 4170–4185 (Article) Subscribed
Publication Date (Web): January 23, 2025

Abstract | Full Text | PDF

ABSTRACT



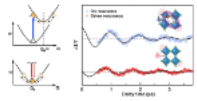
Coherent Exciton Spin Relaxation Dynamics and Exciton Polaron Character in Layered Two-Dimensional Lead-Halide Perovskites

Tingting Qin*, Xiu Zhang, Haijun Liu, Yi Wei, Haijun Huang, Baixu Xiang, Mengdi Zhang, Shaohui Wang, Zhiyong Tang, and Qihua Xiong*

ACS Nano 2025, 19, 4, 4146–4154 (Article) Subscribed
Publication Date (Web): January 22, 2025

Abstract | Full text | PDF

ABSTRACT



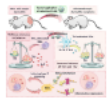
Reductive Adjuvant Nanosystem for Alleviated Atopic Dermatitis Syndromes

Yishao Lu, Xinyu Shan, Jiaxin Huang, Huanli Zhou, Ying Zhu, Jijie Wang, Zhenyu Luo, Xu Liu, Xuemeng Guo, Yingying Shi, Yiling Hu, Huihui Liu, Junlai Zhang, Ping Huang*, Lihua Luo*, and Jian You*

ACS Nano 2025, 19, 4, 4145–4153 (Article) Subscribed
Publication Date (Web): January 22, 2025

Abstract | Full text | PDF

ABSTRACT



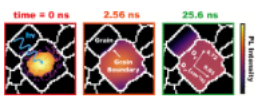
Mapping the Energy Carrier Diffusion Tensor in Perovskite Semiconductors

Roberto Brenes, Dane W. deQuilettes*, Richard Swartwout, Abdullah Y. Alsalloum, Osman M. Bakr, and Vladimir Bulović*

ACS Nano 2025, 19, 4, 4243–4251 (Article) Subscribed
Publication Date (Web): January 17, 2025

Abstract | Full text | PDF

ABSTRACT



ADVERTISEMENT

ON THE PULSE
THE SCIENCE OF SUCCESS
A free science marketing event on Aug. 21, 2025 in DC!
cáen SUMMIT 2025
Learn More

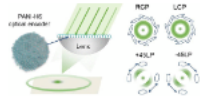
Polarimetric Compressed Sensing with Hollow, Self-Assembled Diffractive Films

Ji Feng, Ariel Perry, Xiaojing Wang, Alma K. Gonzalez-Alcazar, Oriol Arteaga, Maria J. Mendoza, and Luat T. Vuong*

ACS Nano 2025, 19, 4, 4233–4242 (Article) Open Access
Publication Date (Web): January 22, 2025

Abstract | Full text | PDF

ABSTRACT



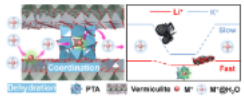
Heteropolyacid Ligands in Two-Dimensional Channels Enable Lithium Separation from Monovalent Cations

Xinyao Dong, Xinyu Ji, Weijun He, Yaming Zhai, Ruiliang Guo, Yi-Wei Li, Zhu-Qing Ma, Yang Yang*, and Kai-De Zhou*

ACS Nano 2025, 19, 4, 4339–4347 (Article) Subscribed
Publication Date (Web): January 9, 2025

Abstract | Full text | PDF

ABSTRACT



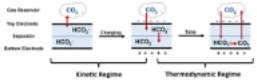
Understanding the Mechanism of Electrochemical CO_2 Capture by Supercapacitive Swing Adsorption

Grace Majestone, Tim M. Kamanga, Zhen Xu, Penelope K. Jones, Alpha S. Lee, Israel Temprano, James Lee, Michael F. L. De Volder, and Alexander C. Forse*

ACS Nano 2025, 19, 4, 4243–4252 (Article) Open Access
Publication Date (Web): January 17, 2025

Abstract | Full text | PDF

ABSTRACT



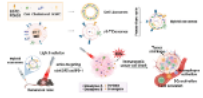
Photosensitive Hybrid γδ-T Exosomes for Targeted Cancer Photoimmunotherapy

Yifan Gao, Jinchao Liu, Meiqen Wu, Yanmei Zhang, Manni Wang, Qingyang Liu, Wenjue Zhang, Yang Zhou, Yin Celeste Cheuk, Xiwei Wang, Yinping Liu, Weiqing Wang*, and Wenwei Tu*

ACS Nano 2025, 19, 4, 4257–4268 (Article) Open Access
Publication Date (Web): January 22, 2025

Abstract | Full text | PDF

ABSTRACT



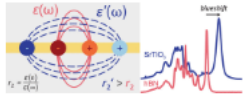
Breakdown of the Static Dielectric Screening Approximation of Coulomb Interactions in Atomically Thin Semiconductors

Amine Ben Mhenni*, Dinh Van Tuan, Leonard Sellier, Marko M. Petrić, Meike Ердl, Kenji Watanabe, Takashi Taniguchi, Seth Ariel Tongay, Kai Müller, Nathan P. Wilson, Jonathan J. Finley*, Hanan Dery, and Matteo Barbone*

ACS Nano 2025, 19, 4, 4269–4279 (Article) Open Access
Publication Date (Web): January 21, 2025

Abstract | Full text | PDF

ABSTRACT



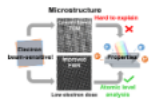
Imaging Electron Beam-Sensitive Twisted Hybrid Perovskite Bilayers at One-Angstrom Resolution

Yuan Lu, Hongcheng Shi, Shuchen Zhang, Daniel Sun, Libai Huang, Letian Dou, and Yi Yu*

ACS Nano 2025, 19, 4, 4279–4288 (Article) Subscribed
Publication Date (Web): January 22, 2025

Abstract | Full text | PDF

ABSTRACT



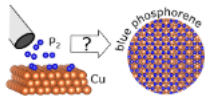
Direct Observation of Structural Phase Transformations during Phosphorene Formation on Cu(111)

Jiří David, František Jaššek, Pavel Procházka, Miroslav Černý, Cristian V. Ciobanu, Stanislav Průša, Tomáš Šikola, Suneel Kodambaka, and Miroslav Kolíbal*

ACS Nano 2025, 19, 4, 4289–4299 (Article) Open Access
Publication Date (Web): January 22, 2025

Abstract | Full text | PDF

ABSTRACT



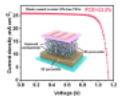
Improved Conductivity of 2D Perovskite Capping Layer for Realizing High-Performance 3D/2D Heterostructured Hole Transport Layer-Free Perovskite Photovoltaics

Si Chen, Wenhuai Feng, Yuxuan Feng, Qing Li, Yu-Hua Huang, Xueqing Chang, Chenying Yao, Yijian Shen, Gengling Liu, Shuang Yang, Xu-Dong Wang, Mingjian Yuan, and Wu-Qiang Wu*

ACS Nano 2025, 19, 4, 4349–4358 (Article) Subscribed
Publication Date (Web): January 24, 2025

Abstract Full text PDF

ABSTRACT



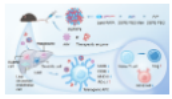
Lipid-Rapamycin Nanovaccines Overcome the Antidrug Antibody Barrier in Biologic Therapies

Xinru Li, Mengyao Ma, Ni Jin, Xiaoxuan Yao, Guzaliinuer Yasen, Mingyuan Zhong, Zheng Jin, Zhonggui He, Yongjun Wang*, and Hongzhuo Liu*

ACS Nano 2025, 19, 4, 4309–4323 (Article) Subscribed
Publication Date (Web): January 24, 2025

Abstract Full text PDF

ABSTRACT



Lattice Anisotropy-Driven Reduction of Phonon Velocities in Black Phosphorus

Prakriti Pradhan Joshi, Dariia Ulrich, Nasim Mirsajjadi, Thomas E. Gage, Luqing Wang, Ruiyu Li, Haihua Liu, Liangbo Liang, Ilke Arslan, Maria K. Y. Chan, and Sarah S. Kong*

ACS Nano 2025, 19, 4, 4300–4308 (Article) Subscribed
Publication Date (Web): January 24, 2025

Abstract Full text PDF

ABSTRACT



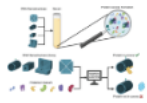
AI-Based Prediction of Protein Corona Composition on DNA Nanostructures

Jared Hulzer, Roxana Coreas, Markita P. Landry, and Grigory Tikhomirov*

ACS Nano 2025, 19, 4, 4289–4302 (Article) Open Access
Publication Date (Web): January 9, 2025

Abstract Full text PDF

ABSTRACT



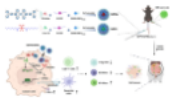
Activating the cGAS-STING Pathway by Manganese-Based Nanoparticles Combined with Platinum-Based Nanoparticles for Enhanced Ovarian Cancer Immunotherapy

Xiangling Zhang, Dongsheng Tang, Haihua Xiao, Bin Li*, Kun Shang*, and Dan Zhao*

ACS Nano 2025, 19, 4, 4269–4288 (Article) Subscribed
Publication Date (Web): January 24, 2025

Abstract Full text PDF

ABSTRACT



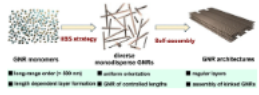
Synthesis and Self-Assembly of Monodisperse Graphene Nanoribbons: Access to Submicron Architectures with Long-Range Order and Uniform Orientation

Jiangfang Yin, Hanfei Wang, Daniel Pyle, Shinyoung Choi, Yusi Liu, Jianguo Wen, Jeffrey R. Guest, Joseph W. Lyding*, and Guanglin Dong*

ACS Nano 2025, 19, 4, 4259–4275 (Article) Subscribed
Publication Date (Web): January 24, 2025

Abstract Full text PDF

ABSTRACT



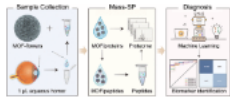
Lanthanide Metal–Organic Framework Flowers for Proteome Profiling and Biomarker Identification in Ultratrace Biofluid Samples

Shuang Zhang, Zhixiao Xu, Youming Chen, Lei Jiang, Jiting Wang, Guangxia Shen, and Wenling Ding*

ACS Nano 2025, 19, 4, 4477–4490 (Article) Subscribed
Publication Date (Web): January 22, 2025

Abstract Full text PDF

ABSTRACT



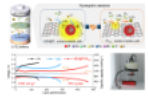
Tuning Dual Catalytic Active Sites of Pt Single Atoms Paired with High-Entropy Alloy Nanoparticles for Advanced Li-O_2 Batteries

Lei Li, Minghao Hua, Jiafeng Li, Peng Zhang, Yingjian Nie, Peng Wang*, Xiaohang Lin, Zhiwei Zhang*, Ruiao Wang, Wenli Ge*, Yuguang C. Li*, and Longwei Yin*

ACS Nano 2025, 19, 4, 4491–4505 (Article) Subscribed
Publication Date (Web): January 17, 2025

Abstract Full text PDF

ABSTRACT



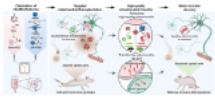
Nanoenzyme-Anchored Mitofactories Boost Mitochondrial Transplantation to Restore Locomotor Function after Paralysis Following Spinal Cord Injury

Rundu Wei, Yiman Chen, Qiang Yang, Tongge Wang, Yanjun He, Na Yin, Liya Yang, Yifei Gao, Ling Guo*, and Min Feng*

ACS Nano 2025, 19, 4, 4459–4501 (Article) Subscribed
Publication Date (Web): January 24, 2025

Abstract Full text PDF

ABSTRACT



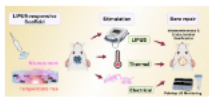
Low-Intensity Pulsed Ultrasound Responsive Scaffold Promotes Intramembranous and Endochondral Ossification via Ultrasonic, Thermal, and Electrical Stimulation

Wanru Jia, Tianlong Wang, Feng Chen*, Zhiqing Liu, Xiaodong Hou, Wentao Cao, Xinyu Zhao, Bingqiang Lu, Yan Hu, Yijie Dong, Jiangtao Zhou*, Zifei Zhou*, and Weiwei Zhan*

ACS Nano 2025, 19, 4, 4429–4439 (Article) Subscribed
Publication Date (Web): January 21, 2025

Abstract Full text PDF

ABSTRACT



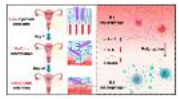
Lactobacillus-Loaded Easily Injectable Hydrogel Promotes Endometrial Repair via Long-Term Retention and Microenvironment Modulation

Guoqing Fan, Yuheng Lu, Yubin Li, Jian Zhang, Yuanbin Wang, Pingyin Lee, Gangyan Zhou, Rongkang Huang*, Binghua Ma*, and Yuan Yuan*

ACS Nano 2026, 19, 4, 4462–4481 (Article) Subscribed
Publication Date (Web): January 17, 2026

Abstract Full text PDF

ABSTRACT



Interfacial Elemental Analysis of Slanted Edge-Contacted Monolayer MoS_2 Transistors via Directionally Angled Etching

Chia-Chun Lin, Naomi Taboulong Reylaga, Chun-Chieh Yen, Yu-Hsuan Lin, Kuang-Hsu Wang, Kenji Watanabe, Takashi Taniguchi, Chi-Te Liang, Shao-Yu Chen, and Wei-Hua Wang*

ACS Nano 2026, 19, 4, 4482–4491 (Article) Open Access
Publication Date (Web): January 21, 2026

Abstract Full text PDF

ABSTRACT



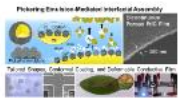
Scalable Fabrication of Freestanding Jammed Nanoparticle Films via Pickering Emulsion-Mediated Interfacial Assembly

Jiwon Heo, Seunghwan Seo, Jusyoung Lee, and Kang Hee Ku*

ACS Nano 2026, 19, 4, 4483–4473 (Article) Subscribed
Publication Date (Web): January 24, 2026

Abstract Full text PDF

ABSTRACT



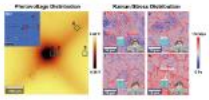
Correlative Raman–Voltage Microscopy Revealing the Localized Structure–Stress Relationship in Silicon Solar Cells

Tianyu Lan, Tianyi Zhao, Yan Liu, Jingyu Cao, Wangli Li, Jie Yang, Xinyu Zhang, Yusheng Wang*, and Baoquan Sun*

ACS Nano 2026, 19, 4, 4473–4483 (Article) Subscribed
Publication Date (Web): January 24, 2026

Abstract Full text PDF

ABSTRACT



Weak H-Bond Interface Environment for Stable Aqueous Zinc Batteries

Shuai Wang, Haoran Wang, Jiguo Tu, Lei Huang, Shenzhen Deng, Bingang Xu*, and Lei Wei*

ACS Nano 2026, 19, 4, 4484–4495 (Article) Subscribed
Publication Date (Web): January 21, 2026

Abstract Full text PDF

ABSTRACT



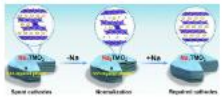
Water-Induced Integrated Regeneration of Cathode Materials from Spent Sodium-Ion Batteries

Youshen Hao, Jinze Guo, Wen Liu, Xiaochong Zhou, Ziqi Tian, Zhongcai Zhang, Yang Lin, Xuan Zhang*, and Yinshu Jiang*

ACS Nano 2026, 19, 4, 4496–4504 (Article) Subscribed
Publication Date (Web): January 24, 2026

Abstract Full text PDF

ABSTRACT



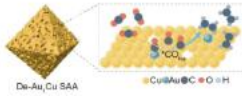
Gold Single Atom Doped Defective Nanoporous Copper Octahedrons for Electrocatalytic Reduction of Carbon Dioxide to Ethylene

Yang Zhao, Yanan Wang, Zhipeng Yu, Chao Song, Jingwei Wang, Haoliang Huang, Lijian Meng, Miao Liu*, and Lifeng Liu*

ACS Nano 2026, 19, 4, 4505–4516 (Article) Subscribed
Publication Date (Web): January 24, 2026

Abstract Full text PDF

ABSTRACT



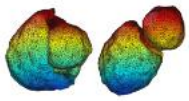
Confinement Induces Morphological and Topological Transitions in Multivesicles

Luis S. Mayorga, Maria L. Mascotti, Bart M. H. Bruininks, and Diego Masone*

ACS Nano 2026, 19, 4, 4517–4527 (Article) Subscribed
Publication Date (Web): January 21, 2026

Abstract Full text PDF

ABSTRACT



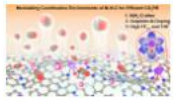
Modulating the Coordination Environment of Atomically Dispersed Nickel for Efficient Electrocatalytic CO_2 Reduction at Low Overpotentials and Industrial Current Densities

Yishen Sun, Xiaolu Liu, Jiasheng Tian, Zixuan Zhang, Yang Li, Yinghui Xie, Mengjie Hao, Zhongshan Chen, Hui Yang*, Geoffrey I. N. Waterhouse, Shengqian Ma*, and Xiangke Wang*

ACS Nano 2026, 19, 4, 4528–4540 (Article) Subscribed
Publication Date (Web): January 24, 2026

Abstract Full text PDF

ABSTRACT



Biofluid-Permeable and Erosion-Resistant Wireless Neural-Electronic Interfaces for Neurohomeostasis Modulation

Zhidong Wei, Fei Jin, Tang Li, Yuyuan He, Lili Qian, Juan Ma, Tao Yuan, Xin Yu, Weiying Zheng, Nagar Jeanmarat, Esteban Pena-Pintos, Ting Wang*, Jianda Xu*, and Zhang-Qi Feng*

ACS Nano 2026, 19, 4, 4541–4560 (Article) Subscribed
Publication Date (Web): January 17, 2026

Abstract Full text PDF

ABSTRACT



Biofluid-Permeable and Erosion-Resistant Wireless Neural-Electronic Interfaces for Neurohomeostasis Modulation

Zhidong Wei, Fei Jin, Tong Li, Yuyuan He, Lili Qian, Juan Ma, Tao Yuan, Xin Yu, Weiying Zheng, Negar Javanmardi, Esteban Pena-Pitrach, Ting Wang*, Jiande Xu*, and Zheng-Qi Feng*

ACS Nano 2025, 19, 4, 4541–4560 (Article) Subscribed
Publication Date (Web): January 17, 2025

Abstract | Full text | PDF

ABSTRACT



Prussian Blue Nanozyme Featuring Enhanced Superoxide Dismutase-like Activity for Myocardial Ischemia Reperfusion Injury Treatment

Mengmeng Long, Limiao Wang, Lina Kang, Songfang Liu, Tingting Long, He Ding, Yifan Duan, Hongliang Han, Biao Xu*, and Ning Gu*

ACS Nano 2025, 19, 4, 4561–4581 (Article) Subscribed
Publication Date (Web): January 21, 2025

Abstract | Full text | PDF

ABSTRACT



Engineered Extracellular Vesicles Modified by Angiopep-2 Peptide Promote Targeted Repair of Spinal Cord Injury and Brain Inflammation

Guang Kong, Jie Liu, Juan Wang, Xiaohu Yu, Gang Li, Mingjiang Deng, Minhao Liu, Siming Wang, Chunming Tang*, Wu Jiang*, and Jin Fan*

ACS Nano 2025, 19, 4, 4583–4600 (Article) Open Access
Publication Date (Web): January 24, 2025

Abstract | Full text | PDF

ABSTRACT



Hydrogen Bond-Driven Hierarchical Assembly of Single-Walled Carbon Nanotubes for Ultrahigh Textile Capacity

Jung Hoon Kim, Ki Su Song, Youngnan Kim, Joon Young Cho, Kyunbae Lee, Do Geun Lee, Joo Hwan Jin, Jungmo Kim, Jong Hwan Park, Wi Hyoung Lee*, Taehoon Kim*, and Joong Tark Han*

ACS Nano 2025, 19, 4, 4601–4613 (Article) Subscribed
Publication Date (Web): January 23, 2025

Abstract | Full text | PDF

ABSTRACT



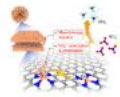
Highly Accessible Electrocatalyst with *In Situ* Formed Copper-Cluster Active Sites for Enhanced Nitrate-to-Ammonia Conversion

Zhen Shen, Fengfei Xu, Xueyi Cheng, Jiatao Jiang, Changkai Zhou, Yu Zang, Xi-Cheng Wang, Lijun Yang, Qiang Wu*, and Sheng Hu*

ACS Nano 2025, 19, 4, 4611–4621 (Article) Subscribed
Publication Date (Web): January 22, 2025

Abstract | Full text | PDF

ABSTRACT



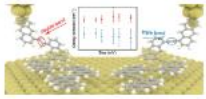
Identifying Carbon−Carbon Triple Bonds from Double Bonds via Single-Molecule Conductance

Jiffan You, Yixuan Gao, Yanning Tang, Chaojie Xu, Jing He, Xiaohao Li, Haiming Zhang, Shikuan Sun*, and Lifang Chi*

ACS Nano 2025, 19, 4, 4629–4638 (Article) Subscribed
Publication Date (Web): January 14, 2025

Abstract | Full text | PDF

ABSTRACT



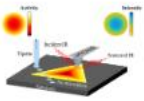
Radially Distributed Electron Transfer on Single-Crystalline Surface of Gold Microplates

Yingjian Li, Huaxu Zhou, Xiaoli Deng, Cong Gao, Li Shen, and Qianjin Chen*

ACS Nano 2025, 19, 4, 4639–4649 (Article) Subscribed
Publication Date (Web): January 21, 2025

Abstract | Full text | PDF

ABSTRACT



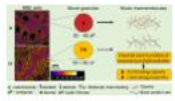
Nanoscale Viscometry Reveals an Inherent Mucus Defect in Cystic Fibrosis

Olga Ponomarchuk, Pranoti Boudreault, Ignacy Gryczynski, Song Lee, Sergei V. Dzyuba, Rafal Fudala, Zygmunt Gryczynski*, John W. Hanrahan, and Ryszard Grygorczyk*

ACS Nano 2025, 19, 4, 4697–4708 (Article) Subscribed
Publication Date (Web): January 14, 2025

Abstract | Full text | PDF

ABSTRACT



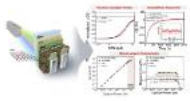
Enhancing Dynamic Range in Low-Noise 2D-Integrated Organic Photodiodes by Mitigating Langevin Recombination

Seung Min Lee, Tae Kyuk Kim, Seyoung Ham, Min Jong Lee, Seunghyun Oh, Yelim Kang, Hyungju Ahn, Hojukng Cha, Seunglun Chung, and Jae Won Shim*

ACS Nano 2025, 19, 4, 4820–4840 (Article) Subscribed
Publication Date (Web): January 22, 2025

Abstract | Full text | PDF

ABSTRACT



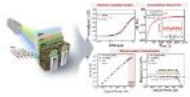
Enhancing Dynamic Range in Low-Noise 2D-Integrated Organic Photodiodes by Mitigating Langevin Recombination

Byeong Min Lee, Tae Hyuk Kim, Geyoung Ham, Min Jong Lee, Seunghyun Oh, Yelim Kang, Hyungju Ahn, Hyojung Cha, Seunghun Chung, and Jae Won Shim*

ACS Nano 2025, 19, 4, 4420–4433 (Article) Subscribed
Publication Date (Web): January 22, 2025

Abstract | Full text | PDF

ABSTRACT



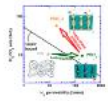
Atomically Fine-Tuning Organic–Inorganic Carbon Molecular Sieve Membranes for Hydrogen Production

Leiqing Hu, Yoon-il Lee, Kai Chen, Soumyabrata Roy, Kieran Fung, Kim Kisslinger, Erda Wang, Yifu Ding, Pulickel M. Ajayan, Chang-Yong Nam*, and Haiqing Lin*

ACS Nano 2025, 19, 4, 4449–4471 (Article) Subscribed
Publication Date (Web): January 20, 2025

Abstract | Full text | PDF

ABSTRACT



Extracellular Matrix-Inspired Dendrimer Nanogels Encapsulating Cyclophosphamide for Systemic Sclerosis Treatment

Junjie Lu, Danqing Huang, Rui Liu, Haofang Zhu, Dandan Wang*, Yuanjin Zhao*, and Lingyun Sun*

ACS Nano 2025, 19, 3, 4479–4499 (Article) Subscribed
Publication Date (Web): January 21, 2025

Abstract | Full text | PDF

ABSTRACT



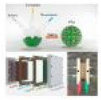
Efficient Nitrate to Ammonia Conversion on Bifunctional $IrCu_4$ Alloy Nanoparticles

Ning He, Zhi Yuan, Chao Wu, Shibo Xi, Jingjing Xiong, Yuzong Huang, Guanru Lian, Zefan Du, Laihao Liu, Daner Wu, Zhongxin Chen*, Wenguang Tu*, Zhigang Zou, and Shuiyin Tong*

ACS Nano 2025, 19, 4, 4489–4499 (Article) Subscribed
Publication Date (Web): January 14, 2025

Abstract | Full text | PDF

ABSTRACT



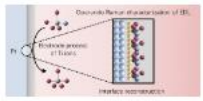
A Deep Insight into the Microscopic Dynamics of the Electrode–Electrolyte Interface under Extreme Operating Conditions

Rui Yuan, Handong Jiao*, Xueyan Du, Leyang Li, Qiang Liu, and Shujiang Jiao*

ACS Nano 2025, 19, 4, 4494–4506 (Article) Subscribed
Publication Date (Web): January 16, 2025

Abstract | Full text | PDF

ABSTRACT



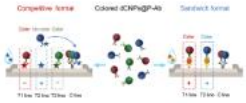
Colored Cellulose Nanoparticles with High Stability and Easily Modified Surface for Accurate and Sensitive Multiplex Lateral Flow Assay

Yizhen Tian, Lei Chen, Xiaodi Liu, Yuying Cheng, Ruisai Xia, Jing Zheng, Yuxia Kang, Yao Gong, Tao Li*, Guodong Wang*, and Qiang Zhang*

ACS Nano 2025, 19, 4, 4709–4717 (Article) Subscribed
Publication Date (Web): January 28, 2025

Abstract | Full text | PDF

ABSTRACT



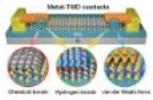
Unraveling the Role of Interfacial Interactions in Electrical Contacts of Atomically Thin Transition-Metal Dichalcogenides

Meiying Gong, Dabao Xie, Yiqian Tian, Zeqi Hua, Congmin Zhang, Meng Li, Dan Cao, Jing Zhou, Xiaozhuang Chen, and Haibo Shu*

ACS Nano 2025, 19, 4, 4719–4730 (Article) Subscribed
Publication Date (Web): January 28, 2025

Abstract | Full text | PDF

ABSTRACT



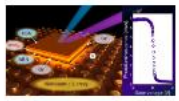
Electrical Control of Photoluminescence in 2D Semiconductors Coupled to Plasmonic Lattices

Antti J. Moilanen, Mohsen Ge(gaël), Takashi Taniguchi, Kenji Watanabe, and Lukas Novotny

ACS Nano 2025, 19, 4, 4741–4748 (Article) Open Access
Publication Date (Web): January 22, 2025

Abstract | Full text | PDF

ABSTRACT



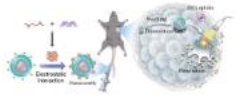
Core–Satellite Nanoassembly Overcomes Spatial Heterogeneity of Dendric Cell Distribution in Pancreatic Tumors for Effective Chemoimmunotherapy

Sengjia Chen, Bo Li, Tan Li, Minzhao Lin, Huihui Zhong, Xiaoxue Xia, Qiaojun Zhang, Qi Chen, Xiaochun Wang*, Zesong Wan*, and Zhirao Shuai*

ACS Nano 2025, 19, 4, 4749–4763 (Article) Subscribed
Publication Date (Web): January 20, 2025

Abstract | Full text | PDF

ABSTRACT



Shape-Directed Dynamic Assembly of Active Colloidal Metamachines

Yang Huang, Ling Yang, Siyang Yang, Hao Chen, Gali Lou, Yunqing Tang, Xiankun Lin*, and Qiang He*

ACS Nano 2025, 19, 4, 4764–4774 (Article) Subscribed
Publication Date (Web): January 24, 2025

Abstract | Full text | PDF

ABSTRACT



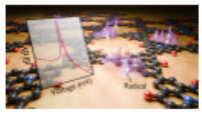
On-Surface Synthesis and Characterization of Radical Spins in Kagome Graphene

Rémy Pawlak*, Khalid N. Sridhya, Guihrmane Chahib, Jung-Ching Liu, Paul Hirel, Laurent Marot, Vincent Luzet, Frank Palmino, Frédéric Chérioux, Alain Rochefort, and Ernst Meyer*

ACS Nano 2025, 19, 4, 4749–4777 (Article) Open Access
Publication Date (Web): January 10, 2025

Abstract | Full text | PDF

ABSTRACT



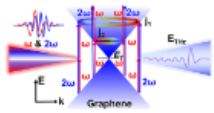
Coherent Photocurrent Injection through Quantum Interference between Stimulated Electronic Raman Scattering and Single-Photon Absorption in Intrinsic Graphene

Yuhang He, Yuxuan Chen, Xiangyu Le, Chenyin Dai, Liangliang Zhang, Zhen Tian*, and Jianming Dai*

ACS Nano 2025, 19, 4, 4774–4784 (Article) Subscribed
Publication Date (Web): January 20, 2025

Abstract | Full text | PDF

ABSTRACT



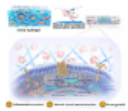
Metabolic Reprogramming of Neural Stem Cells by Chiral Nanofiber for Spinal Cord Injury

Haining Wu, Chao Xing, Saibei Yu, Lingli Guo, Xiaoqiu Dou*, Laiben Gao, Shijie Yang, Yongfeng Zhang, Xue Gao, Shengyou Li, Bing Xia, Teng Ma, Yiming Hao, Yujie Yang, Xueli Gao, Yitao Wei, Gorui Xue, Qing Zhang, Chuan-Hang Feng*, and Jinghui Huang*

ACS Nano 2025, 19, 4, 4749–4801 (Article) Open Access
Publication Date (Web): January 22, 2025

Abstract | Full text | PDF

ABSTRACT



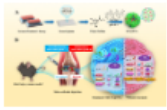
High-Throughput Screening Strategy and Metal–Organic Framework-Based Multifunctional Controlled-Release Nanomaterial for Osteoarthritis Therapy

Yu Chen, Yekai Zhang, Chenyu Wu, Xiaojing Zhao, Hanwen Zhang, Chenzhao Li, Yuxin Deng, Liaojun Sun, Yifei Zhou*, and Xiaolei Zhang*

ACS Nano 2025, 19, 4, 4800–4819 (Article) Subscribed
Publication Date (Web): January 19, 2025

Abstract | Full text | PDF

ABSTRACT



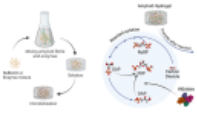
Beyond CO_2 Storage: Enzyme-Amyloid Fibril Catalytic Hybrids for Long Cascade Reactions Converting CO_2 into Fructose

Tonghui Jin, Sophally Chhong, Mingqin Li, Jiangnan Zhou, Qiao Xuan, Jiaqi Su, Ming Dai, Mohammad Peydayesh, Zhou Dong, Qiyao Sun, Mattia Usuelli, and Raffaele Mezzenga*

ACS Nano 2025, 19, 4, 4820–4829 (Article) Subscribed
Publication Date (Web): January 24, 2025

Abstract | Full text | PDF

ABSTRACT



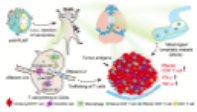
Targeted Modulation of the Meningeal Lymphatic Reverse Pathway for Immunotherapy of Breast Cancer Brain Metastases

Yanfeng Dai, Xiang Yu, Yifan Zhao, Jianshuang Wei, Dong Lin, Jiaju Wang, Ran Zhang, Xuanan Yuan, Sanmu Li, Songlin Huang, Qian Liu*, and Zhihong Zhang*

ACS Nano 2025, 19, 4, 4830–4846 (Article) Subscribed
Publication Date (Web): January 17, 2025

Abstract | Full text | PDF

ABSTRACT



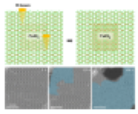
Defect Migration and Phase Transformations in Two-Dimensional Iron Chloride inside Bilayer Graphene

Qiunan Liu, Haiming Sun, Yung-Chang Lin*, Mahdi Ghorbani-Asl, Sihan Kretschmer, Chi-Chun Cheng, Po-Wen Chiu, Hiroki Ago, Arkady V. Krasheninnikov*, and Kazu Suenaga*

ACS Nano 2025, 19, 4, 4847–4854 (Article) Subscribed
Publication Date (Web): January 24, 2025

Abstract | Full text | PDF

ABSTRACT



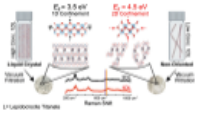
Concentration-Dependent Control of the Band Gap Energy of a Low-Dimensional Lepidocrocite Titanate

Adam D. Walter, Gregory R. Schurenin*, Yuanren Liu, David Bugallo Ferron, Jeffrey T. Wilt, Lucas M. Ferrer, Christopher Y. Li, Yang-Jun Hu, and Michel W. Barsoum*

ACS Nano 2025, 19, 4, 4855–4866 (Article) Open Access
Publication Date (Web): January 16, 2025

Abstract | Full text | PDF

ABSTRACT



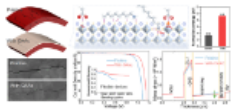
Mechanically Resilient and Highly Efficient Flexible Perovskite Solar Cells with Octylammonium Acetate for Surface Adhesion and Stress Relief

Yumeng Xu, Biyu Zhang, Haidong Yuan, Yong Jiao, Xing Guo, Zhaosheng Hu, Xian-gang Hu, Zhenhua Lin*, Yue Hao, Liming Ding, and Jingjing Chang*

ACS Nano 2025, 19, 4, 4867–4878 (Article) Subscribed
Publication Date (Web): January 22, 2025

Abstract | Full text | PDF

ABSTRACT



Revealing the Water Structure at Neutral and Charged Graphene/Water Interfaces

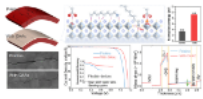
Mechanically Resilient and Highly Efficient Flexible Perovskite Solar Cells with Octylammonium Acetate for Surface Adhesion and Stress Relief

Yumeng Xu, Biyu Zhang, Haidong Yuan, Yong Jiao, Xing Gao, Zhaosheng Hu, Wan-gang Hu, Zhenhua Lin*, Yue Hao, Liming Ding, and Jingling Chang*

ACS Nano 2025, 19, 4, 4367–4375 (Article) Subscribed
Publication Date (Web): January 22, 2025

Abstract | Full Text | PDF

ABSTRACT



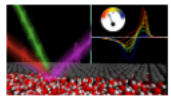
Revealing the Water Structure at Neutral and Charged Graphene/Water Interfaces through Quantum Simulations of Sum Frequency Generation Spectra

Richa Rashmi, Toheeb O. Balogun, Golam Adam, Henry Agnew, Rakesh Kumar*, and Francesco Paesani*

ACS Nano 2025, 19, 4, 4375–4385 (Article) Subscribed
Publication Date (Web): January 21, 2025

Abstract | Full Text | PDF

ABSTRACT



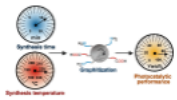
Structure Matters: Tailored Graphitization of Carbon Dots Enhances Photocatalytic Performance

Laura Mortiboni, Lucia Cardo, Elisa Sturabotti, Pierangelo Gobbo*, Giacomo Filippini*, and Maurizio Prato*

ACS Nano 2025, 19, 4, 4387–4400 (Article) Open Access
Publication Date (Web): January 22, 2025

Abstract | Full Text | PDF

ABSTRACT



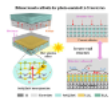
Coupling Bifunctional Scaffolds with Slow Photon Effect for Synergistically Enhanced Photoassisted Lithium–Sulfur Battery Properties

Ting Meng, Xiaohan Wang, Wenbo Zhao, Yong Gao, Zeju Geng, Jiyang Chen, Fan Bu, Haifei Zhu, Junwei Li, Haifeng Zhang*, and Cao Guan*

ACS Nano 2025, 19, 4, 4401–4413 (Article) Subscribed
Publication Date (Web): January 22, 2025

Abstract | Full Text | PDF

ABSTRACT



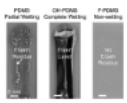
Dynamic-Wetting Liquid Metal Thin Layer Induced via Surface Oxygen-Containing Functional Groups

Yue Zhang, Zhao Wang, Shutong Wang, Zhennai Yu*, Zhe Xu*, and Lei Jiang*

ACS Nano 2025, 19, 4, 4413–4423 (Article) Subscribed
Publication Date (Web): January 22, 2025

Abstract | Full Text | PDF

ABSTRACT



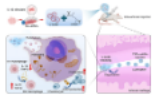
Remodeling the Proinflammatory Microenvironment in Osteoarthritis through Interleukin-1 Beta Tailored Exosome Cargo for Inflammatory Regulation and Cartilage Regeneration

Manyu Chen, Yuhan Liu, Yi Cao, Chengkun Zhao, Guanying Liu, Na Li, Yuan Liu, Xiaolin Cui, Pengcheng Liu, Jia Liang, Yujiang Fan*, Qiguang Wang*, and Xingdong Zhang*

ACS Nano 2025, 19, 4, 4424–4441 (Article) Subscribed
Publication Date (Web): January 23, 2025

Abstract | Full Text | PDF

ABSTRACT



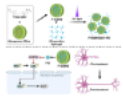
Neuronal Dual-Specificity Phosphatase 26 Inhibition via Reactive-Oxygen-Species Responsive Mesoporous-Silica-Loaded Hydrogel for Spinal Cord Injury Repair

Kai Zhang, Runlin Wan, Wanrong Ma, Xinghui He, Zhiguan Yang, Dingkang Liu*, and Xing Li*

ACS Nano 2025, 19, 4, 4442–4458 (Article) Subscribed
Publication Date (Web): January 23, 2025

Abstract | Full Text | PDF

ABSTRACT



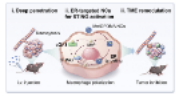
Endoplasmic Reticulum-Targeted Polymer-Manganese Nanocomplexes for Tumor Immunotherapy

Haoru Zhu, Cheng Xu, Yu Geng, Youqing Shen*, and Nasha Qiu*

ACS Nano 2025, 19, 4, 4459–4472 (Article) Subscribed
Publication Date (Web): January 24, 2025

Abstract | Full Text | PDF

ABSTRACT



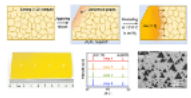
Low-Cost Preparation of Wafer-Scale Au(111) Single Crystals for the Epitaxy of Two-Dimensional Layered Materials

Jingyi Hu, Jialong Wang, Pengfei Yang, Wenzhi Quan, Xuan Wang, Haoxuan Ding, Jiatan Fu, You Peng, Ronghua Zhang, Hongpeng Wang, Liming Xie, Ke He, Lili Wang, Wei Wei, Leining Zhang*, Zhongfan Liu*, and Yanfeng Zhang*

ACS Nano 2025, 19, 4, 4473–4482 (Article) Subscribed
Publication Date (Web): January 24, 2025

Abstract | Full Text | PDF

ABSTRACT



A CRISPR-Cas and Argonaute-Driven Two-Factor Authentication Strategy for Information Security

Ruijie Fu, Jinjie Hou, Jiaxiang Wang, Chenggang Zhu, and Yunlei Xianyu*

ACS Nano 2025, 19, 4, 4483–4492 (Article) Subscribed
Publication Date (Web): January 24, 2025

Abstract | Full Text | PDF

ABSTRACT



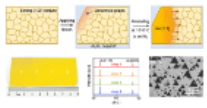
Low-Cost Preparation of Wafer-Scale Au(111) Single Crystals for the Epitaxy of Two-Dimensional Layered Materials

Jingyi Hu, Jialong Wang, Pengfei Yang, Wenshi Guan, Xuan Wang, Haoxuan Ding, Jiatian Fu, You Peng, Ronghua Zhang, Hongpeng Wang, Liming Xie, Ke He, Lili Wang, Wei Wei, Leining Zhang*, Zhongfan Liu*, and Yanfeng Zhang*

ACS Nano 2025, 19, 4, 4473–4482 (Article) Subscribed
Publication Date (Web): January 24, 2025

Abstract Full text PDF

ABSTRACT



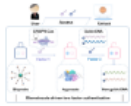
A CRISPR-Cas and Argonaute-Driven Two-Factor Authentication Strategy for Information Security

Rujia Fu, Jinjie Hou, Zexiang Wang, Chenggang Zhu, and Yunkai Xiang*

ACS Nano 2025, 19, 4, 4483–4492 (Article) Subscribed
Publication Date (Web): January 24, 2025

Abstract Full text PDF

ABSTRACT



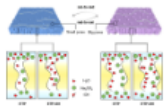
Pulsatile Ion Transport in Nanofiltration Membranes Coupled with Electrically Tunable Pore and Hydroxyl Electrostatic Interactions

You Wu, Zhibin Chen, Chenghai Lu, Chengzhi Hu*, and Jiuhui Qu

ACS Nano 2025, 19, 4, 4493–4504 (Article) Subscribed
Publication Date (Web): January 24, 2025

Abstract Full text PDF

ABSTRACT



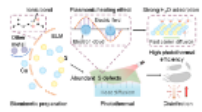
Biomimetic Confined Assembly of Plasmonic CuS from Electronic Waste for Rapid Photothermal Disinfection

Zeinel Hao, Jingyu Sun, Jiabin Chen*, Yinchuan Yang, Xiaoqi Sun, Ruiqiang Ji, Qiang Zhao, Xuefei Zhou, Hongbo Zeng, and Yalei Zhang*

ACS Nano 2025, 19, 4, 4505–4514 (Article) Subscribed
Publication Date (Web): January 17, 2025

Abstract Full text PDF

ABSTRACT



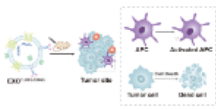
EXO$^{TLR1/2\text{-}STING}$: A Dual-Mechanism Stimulator of Interferon Genes Activator for Cancer Immunotherapy

Tian-Yang Wang, Hong-Guo Hu, Lang Zhao, Shao-Hua Zhou, JingYun Su, Geng-Hui Feng, and Yan-Mei Li*

ACS Nano 2025, 19, 4, 4515–4536 (Article) Subscribed
Publication Date (Web): January 22, 2025

Abstract Full text PDF

ABSTRACT



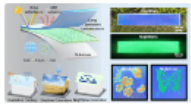
Hierarchical Nanocellulose Photonic Design for Synergistic Colored Radiative Cooling

Yi Zhou, Canhui Lu*, and Rui Xiong*

ACS Nano 2025, 19, 4, 4537–4549 (Article) Subscribed
Publication Date (Web): January 22, 2025

Abstract Full text PDF

ABSTRACT



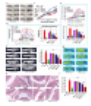
ADDITIONS AND CORRECTIONS

Correction to "Biomimetic Hybrid Membrane-Coated Xuetongsu Assisted with Laser Irradiation for Efficient Rheumatoid Arthritis Therapy"

Huanghe Yu, Jialong Fan, Nushet Sheila, Yixing Qiu, Ye Lin, Zhou Wang, Liang Cao, Bin Li, Muhammad Daniyal, Yan Qin, Caijun Peng, Xiang Cai*, Bin Liu*, and Wei Wang*

ACS Nano 2025, 19, 4, 4543–4543 (Addition/Correction) Subscribed
Publication Date (Web): January 24, 2025

First Page Full text PDF

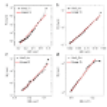


Correction to "Fermi Level Pinning at Electrical Metal Contacts of Monolayer Molybdenum Dichalcogenides"

Changeik Kim, Inyong Moon, Daeyeong Lee, Min Sup Choi, Faisal Ahmed, Seunggeol Nam, Yeonchoo Cho, Hyeon-Jin Shin, Seongjun Park, and Won Jong Yoo*

ACS Nano 2025, 19, 4, 4549 (Addition/Correction) Subscribed
Publication Date (Web): January 22, 2025

First Page Full text PDF



MASTHEADS

Issue Editorial Masthead

ACS Nano 2025, 19, 4, 3001–3001 (Article) Subscribed
Publication Date (Web): February 4, 2025

First Page PDF

Issue Publication Information

ACS Nano 2025, 19, 4, 3001–3001 (Article) Subscribed
Publication Date (Web): February 4, 2025

First Page PDF

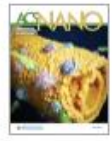
Archive of 2025 Online Issues



June 3, 2025 | Vol. 19 Issue 21
pp. 19509-20269
CURRENT ISSUE



May 27, 2025 | Vol. 19 Issue 20
pp. 18889-19508



May 20, 2025 | Vol. 19 Issue 19
pp. 17953-18888



May 13, 2025 | Vol. 19 Issue 18
pp. 17041-17952



May 6, 2025 | Vol. 19 Issue 17
pp. 16193-17040



April 29, 2025 | Vol. 19 Issue 16
pp. 15173-16192



April 22, 2025 | Vol. 19 Issue 15
pp. 14521-15172



April 15, 2025 | Vol. 19 Issue 14
pp. 13491-14520



April 8, 2025 | Vol. 19 Issue 13
pp. 12427-13490



April 1, 2025 | Vol. 19 Issue 12
pp. 11465-12426



March 25, 2025 | Vol. 19 Issue 11
pp. 10579-11464



March 18, 2025 | Vol. 19 Issue 10
pp. 9435-10578



March 11, 2025 | Vol. 19 Issue 9
pp. 8381-9434



March 4, 2025 | Vol. 19 Issue 8
pp. 7417-8380



February 25, 2025 | Vol. 19 Issue 7
pp. 6613-7416



February 18, 2025 | Vol. 19 Issue 6
pp. 5861-6612



February 11, 2025 | Vol. 19 Issue 5
pp. 5045-5860



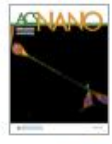
February 4, 2025 | Vol. 19 Issue 4
pp. 3967-5044



January 28, 2025 | Vol. 19 Issue 3
pp. 2977-3966



January 21, 2025 | Vol. 19 Issue 2
pp. 1861-2976



January 14, 2025 | Vol. 19 Issue 1
pp. 1-1860

MASTHEADS

Issue Editorial Masthead

ACS Nano 2025, 19, 4, XXX-XXX **(Article)** Subscribed
Publication Date (Web): February 4, 2025

First Page PDF

Issue Publication Information

ACS Nano 2025, 19, 4, XXX-XXX **(Article)** Subscribed
Publication Date (Web): February 4, 2025

First Page PDF

ers Atypon CHORUS COPE COUNTER Crossref Crossref Similarity Check ORCID Connecting Research and Researchers PORTICO

ACS Publications
Most Trusted. Most Cited. Most Read.

1155 Sixteenth Street N.W.
Washington, DC 20036
Copyright © 2025
American Chemical Society

About
About ACS Publications
ACS & Open Access
ACS Membership
ACS Publications Blog

Resources and Information
Journals A-Z
Books and Reference
Advertising Media Kit
Institutional Sales
ACS Researcher Resources
ACS Publishing Center
Privacy Policy
Terms of Use

Support & Contact
Help
Live Chat
FAQ

Connect with ACS Publications

ACSNANO

EDITOR-IN-CHIEF: XIAODONG CHEN
Nanyang Technological University, Singapore
eic@nano.acs.org

EXECUTIVE EDITORS

Jillian Buriak
University of Alberta, Canada
buriak-office@nano.acs.org

Warren C.W. Chan
University of Toronto, Canada
chan-office@nano.acs.org

Chunying Chen
National Center for Nanoscience and Technology, China
chenchy-office@nano.acs.org

Mark Hersam
Northwestern University, United States
hersam-office@nano.acs.org

Il-Doo Kim
Korea Advanced Institute of Science and Technology, Republic of Korea
kim-office@nano.acs.org

Yan Li
Peking University, China
li-office@nano.acs.org

Luis Liz-Marzán
CIC biomaGUNE, Spain
liz-marzan-office@nano.acs.org

ASSOCIATE EDITORS

Deji Akinwande
University of Texas at Austin, United States
akinwande-office@nano.acs.org

Natalie Artzi
Harvard Medical School, United States
artzi-office@nano.acs.org

Sara Bals
Antwerp University, Belgium
bals-office@nano.acs.org

Jeffrey Brinker
University of New Mexico, United States
brinker-office@nano.acs.org

Yang Chai
The Hong Kong Polytechnic University, Hong Kong
chai-office@nano.acs.org

Lifeng Chi
Soochow University, China
chi-office@nano.acs.org

Denis Ho
National University of Singapore, Singapore
ho-office@nano.acs.org

Anita Ho-Baillie
University of Sydney, Australia
ho-baillie-office@nano.acs.org

Liangbing Hu
University of Maryland, United States
hu-office@nano.acs.org

Tony Hu
Tulane University, United States
hu-office@nano.acs.org

Yu Huang
University of California Los Angeles, United States
huang-office@nano.acs.org

Ana Jaklenec
Massachusetts Institute of Technology, United States
jaklenec-office@nano.acs.org

Kazunori Kataoka
University of Tokyo, Japan
kataoka-office@nano.acs.org

Young Hee Lee
Sungkyunkwan University, Republic of Korea
young-office@nano.acs.org

Maria Lukatskaya
ETH Zürich, Switzerland
lukatskaya-office@nano.acs.org

Matthew McDowell
Georgia Institute of Technology, United States
mcdowell-office@nano.acs.org

Jill Millstone
University of Pittsburgh, United States
millstone-office@nano.acs.org

Prineha Narang
University of California Los Angeles, United States
narang-office@nano.acs.org

Rahmi Oklu
Mayo Clinic, United States
oklu-office@nano.acs.org

Wolfgang Parak
Universität Hamburg, Germany
parak-office@nano.acs.org

Mathieu Salanne
Sorbonne University, France
salanne-office@nano.acs.org

Paolo Samorì
University of Strasbourg, France
samori-office@nano.acs.org

Raymond E. Schaak
The Pennsylvania State University, United States
schaak-office@nano.acs.org

Tsuyoshi Sekitani
Osaka University, Japan
sekitani-office@nano.acs.org

Berend Smit
Ecole Polytechnique Fédérale de Lausanne, Switzerland
smit-office@nano.acs.org

Ajay K. Sood
Indian Institute of Science, India
sood-office@nano.acs.org

Bozhi Tian
University of Chicago, United States
tian-office@nano.acs.org

Ilja K. Voets
Eindhoven University of Technology, Netherlands
voets-office@nano.acs.org

Shutao Wang
Technical Institute of Physics and Chemistry Chinese Academy of Sciences, China
wang-office@nano.acs.org

Katherine A. (Kallie) Willets
Temple University, United States
willets-office@nano.acs.org

Huolin Xin
University of California Irvine, United States
xin-office@nano.acs.org

Jinhua Ye
Hebei University, China
ye-office@nano.acs.org

MANAGING EDITOR
managing.editor@nano.acs.org

EDITORIAL ADVISORY BOARD

Kristi S. Anseth
University of Colorado, United States

Chunli Bai
Chinese Academy of Sciences, China

Zhenan Bao
Stanford University, United States

Frank Bates
University of Minnesota, United States

Thomas Bein
Ludwig-Maximilians-Universität München, Germany

Carolyn R. Bertozzi
Stanford University, United States

Flemming Besenbacher
University of Aarhus, Denmark

Sangeeta Bhatia
Massachusetts Institute of Technology, United States

Marcella Bonchio
University of Padova, Italy

Frank Caruso
University of Melbourne, Australia

Xiaoyuan (Shawn) Chen
National University of Singapore, Singapore

Hui-Ming Cheng
Tsinghua University, China

Samuel Chigome
Botswana Institute for Technology Research and Innovation, Botswana

Jonathan Coleman
Trinity College Dublin, Ireland

Emiliano Cortés
Ludwig Maximilians University Munich, Germany

Kenneth A. Dawson
University College Dublin, Ireland

Cees Dekker
Delft University of Technology, Netherlands

Mostafa A. El-Sayed
Georgia Institute of Technology, United States

Chunhai Fan
Shanghai Jiao Tong University, China

Omid Farokhzad
Harvard Medical School, United States

Christoph Gerber
University of Basel, Switzerland

David S. Ginger
University of Washington, United States

Yury Gogotsi
Drexel University, United States

Naomi J. Halas
Rice University, United States

Christy L. Haynes
University of Minnesota, United States

Chris Hogan
University of Minnesota, United States

Darrell J. Irvine
Massachusetts Institute of Technology, United States

Chennupati Jagadish
Australian National University, Australia

Lei Jiang
Beihang University, China

Kourosh Kalantar-Zadeh
University of Sydney, Australia

Sergei Kalinin
Oak Ridge National Laboratory, United States

Shana O. Kelley
Northwestern University, United States

Laura L. Kiessling
Massachusetts Institute of Technology, United States

Andreas Kis
EPFL, Switzerland

Rafal Klajn
Weizmann Institute of Science, Israel

Kostas Kostarelos
University of Manchester, United Kingdom

Christy Landes
Rice University, United States

Katharina Landfester
Max Planck Institute for Polymer Research, Germany

Taikjoo Lee
Seoul National University, Republic of Korea

Graham Leggett
University of Sheffield, United Kingdom

Xing-Jie Liang
National Center for Nanoscience and Technology of China, China

Bin Liu
National University of Singapore, Singapore

Gang-yu Liu
University of California, Davis, United States

Zhongfan Liu
Peking University, China

Chad A. Mirkin
Northwestern University, United States

Catherine J. Murphy
University of Illinois at Urbana-Champaign, United States

Ki Tae Nam
Seoul National University, Republic of Korea

Teri W. Odom
Northwestern University, United States

Aydogan Ozcan
University of California, Los Angeles, United States

Richard E. Palmer
Swansea University, United Kingdom

Nicholas A. Peppas
University of Texas at Austin, United States

Maurizio Prato
University of Trieste, Italy

Martin Pumera
Central European Institute of Technology, Czech Republic

C. N. R. Rao
CSIR Center for Excellence in Chemistry, India

John A. Rogers
Northwestern University, United States

Michael J. Sailor
University of California, San Diego, United States

Lars Samuelson
Lund University, Sweden

Edward (Ted) Sargent
University of Toronto, Canada

Molly S. Shoichet
University of Toronto, Canada

Michelle Simmons
University of New South Wales, Australia

Zuzanna S. Siwy
University of California, Irvine, United States

Sara E. Skrabalak
Indiana University, United States

Byeong-Hyeok Sohn
Seoul National University, Republic of Korea

Nicole F. Steinmetz
University of California San Diego, United States

Ben Zhong Tang
The Hong Kong University of Science & Technology, China

Joseph Wang
University of California, San Diego, United States

Zhong Lin Wang
Georgia Institute of Technology, United States

Jamie Warner
University of Texas at Austin, United States

Tanja Weil
Max Planck Institute for Polymer Research, Germany

Claire Wilhelm
Curie Institute, France

Itamar Willner
Hebrew University of Jerusalem, Israel

Jiao-Bin Xu
Chinese University of Hong Kong, China

Vivian W. W. Yam
University of Hong Kong, China

Jackie Ying
*Agency for Science, Technology and Research (A*STAR), Singapore*

Zhong Yu
Jilin University, China

Haitao (Alice) Zhang
Peking University, China

Hua Zhang
City University of Hong Kong, China

Yuliang Zhao
National Center for Nanoscience and Technology of China, China

Chongwu Zhou
University of Southern California, United States

ACS NANO

ACS Nano (ISSN 1936-0851) is published weekly except for the first week in January by the American Chemical Society at 1155 16th St. NW, Washington, DC 20036.

American Chemical Society
1155 16th St. NW, Washington, DC 20036
(202) 872-4600; TDD (202) 872-6076; Fax (202) 776-8264

Customer Service & Information
https://acs.service-now.com/acs Tel (202) 872-4376
Email support@services.acs.org

Global Production Operations
American Chemical Society
2540 Olentangy River Road
P.O. Box 3330, Columbus, OH 43210
(614) 447-3665; Fax (614) 447-3745
Email acsproof@acs.org

ACS Publications Advertising Office
1155 16th St. NW, Washington, DC 20036
(202) 872-4536; Email advertising@acs.org

Global Sales and Support
(614) 447-3674; (888) 338-0012; ACS_Pubs_Assist@acs.org
For ACS products and access options, visit https://solutions.acs.org/

Publications Division
James Milne, President

Journals Publishing Group
Sarah B. Tegen, Senior Vice President, Chief Publishing Officer

Global Editorial Strategy
Teodoro Pulvirenti, Senior Director
Paul-André Genest, Publisher
Sai Konda, Associate Publisher
Sergey Shmakov, Managing Editor

Global Editorial Operations
Beth Crannen, Senior Director
Heather Demke, Assistant Director, Editorial Services
Angela Hunter, Manager, Publishing Integrity Office

Global Production Operations
John W. Blanchard, Senior Director
Leslie A. Walker, Director, Technical Editing
Mark J. Wyatt, Senior Editor

Product Management
Norma Cernadas, VP, Product Management
Jessica Rucker, Senior Director, Product Strategy & Operations
Anthony Apodaca, Director, Publishing Platforms
Jeff Lang, Director, Engagement Platforms
Allison Leung, Director, Academia Products & Services

Global Marketing and Community Development
Matthew Chan, Vice President, Global Marketing, Community Development & Communications
Ellie Key, Director, Product Marketing - Journals
Jennifer Winders, Senior Marketing Manager
Shane Lo Maglio, Marketing Manager

Copyright Permission: To reuse figures, tables, artwork, illustrations, and text from articles in this journal that are only available through a subscription, ACS requests that interested parties use the Copyright Clearance Center RightsLink service. The terms of use for open access articles in this journal are marked with a CC-BY or CC-BY-NC-ND license; those licenses link to the appropriate permissions and terms of use.

Instructions for Authors:
Visit the ACS website (https://researcher-resources.acs.org/publish/). Please conform to these instructions when submitting manuscripts.

ACS Journal Publishing Agreement:
After their article is accepted by an ACS journal and before it is published, authors are required to sign an ACS Journal Publishing Agreement. Visit https://pubs.acs.org/page/copyright/journals/jpa_index.html for more information about the ACS Journal Publishing Agreement options.

Manuscript Submission:
Submit via the Journal Website (https://pubs.acs.org/journal/ancac3).

Accepted Papers and Proofs:
Direct correspondence to Global Production Operations (see above).

Journal Policies:
The American Chemical Society and its Editors assume no responsibility for the statements and opinions advanced by contributors. Registered names and trademarks, etc., used in this publication, even without specific indication thereof, are not to be considered unprotected by law.

Subscription and Ordering Information:
Institutional subscribers may contact Global Sales and Support (see above) for web and print subscription information.

Digital Object Identifier (DOI):
The DOI identification system for digital media has been designed to provide persistent and reliable identification of digital objects. Information on the DOI and its governing body, the International DOI Foundation, can be found at http://www.doi.org. The DOI is prominently displayed on each published paper.

Claims for Issues Not Received:
Claims will be honored only if submitted within 90 days of the issue date for subscribers in North America or within 180 days of the issue date for all other subscribers. Contact Customer Billing & Account Support. Tel (614) 447-3674 or (888) 338-0012; Fax (614) 447-5475; Email Liblink@acs.org.

Back Issue Orders:
To order print copies of issues from January 2010 forward, contact Global Sales and Support at ACS_Pubs_Assist@acs.org.

Bulk Reprint Orders:
For information on ordering commercial reprints, contact Global Sales and Support at ACS_Pubs_Assist@acs.org.

Supporting Information (SI):
Supporting Information, if provided, is published with each article online and available free of charge by visiting pubs.acs.org and navigating to the article.

Terms of Use:
The terms of use for articles in this journal that are only available through a subscription shall be governed by applicable institutional agreements. The terms of use for open access articles in this journal are marked with a CC-BY or CC-BY-NC-ND license; those licenses link to the appropriate terms of use.

Canadian GST Reg. No. 127571347

© Copyright 2025 American Chemical Society

SCI 论文专家鉴定意见

兹证明论文《CorrelativeRaman-VoltageMicroscopy RevealingtheLocalizedStructure-Stress RelationshipinSiliconSolarCells》为苏州大学纳米科学技术学院本科生赵天翊（学号 2209401081）的学术成果、该成果与纳米材料与技术专业有较强的相关性。

申请人签名：赵天翊

证明老师签名：

2025 年 6 月 4 日

创新创业学分认定诚信声明

本人郑重声明：所提交的用以申请创新创业学分认定的内容（包括但不限于学科竞赛获奖、学术论文、科研项目成果、专利创造成果、文学艺术类成果以及创业实践类成果等）均为本人在校期间原创取得，不存在任何侵权、造假等违规行为。

本人完全意识到本声明的法律后果由本人承担。本人所提交的内容如涉嫌违规违法，本人愿意承担相应后果。

申请人签名：赵天阳

指导（证明）老师签名：

2024年6月 4日